Ore Geology Reviews 145 (2022) 104912

Contents lists available at ScienceDirect

Ore Geology Reviews

journal homepage: www.elsevier.com/locate/oregeorev

Genesis and high-pressure evolution of the Köyceğiz ophiolite (SW Turkey): Mineralogical and geochemical characteristics of podiform chromitites

Fahui Xiong [a,b,*], Basem Zoheir [c,d,*], Xiangzhen Xu [a,b], Davide Lenaz [e], Jingsui Yang [a,b]

[a] Center for Advanced Research on the Mantle (CARMA), Key Laboratory of Deep-Earth Dynamics of Ministry of Natural Resources, Institute of Geology, Chinese Academy of Geological Sciences, Beijing 100037, China
[b] Southern Marine Science and Engineering Guangdong Laboratory (Guangzhou), Guangzhou 511458, China
[c] Department of Geology, Faculty of Science, Benha University, 13518 Benha, Egypt
[d] Institute of Geosciences, University of Kiel, Ludewig-Meyn Str. 10, 24118 Kiel, Germany
[e] Department of Mathematics and Earth Sciences, University of Trieste, Via Weiss 8, 34128 Trieste, Italy

ARTICLE INFO

Keywords:
Köyceğiz chromitites
UHP-SuR mineral inclusions
Lamellar silicate inclusions
Mantle recycling
Supra-subduction zone ophiolites

ABSTRACT

Textural and compositional characteristics of mineral inclusions in podiform chromitites flourish thoughtful information about the genesis of the Köyceğiz ophiolite (SW Turkey). In the chromitite bodies, olivine, orthopyroxene, clinopyroxene, and sulfide inclusions are mostly sub-rounded or globular. Less abundant needle-shaped silicate inclusions (10–50 μm-long) are aligned along crystallographic orientations in the host magnesiochromite grains. Raman spectroscopy and micro analytical data indicate that these lamellar inclusions have consistently a diopside composition. Uncommon, discrete micro-diamonds and moissanite (SiC) particles, observed in some magnesiochromite grains, may suggest formation under ultra-high pressure (UHP) super-reduced (SuR) conditions.

The Köyceğiz chromitites are characterized by variable platinum-group element (PGE) abundances (80–441 ppb), with unfailing IPGE > PPGE contents. Fractionated chondrite-normalized PGE patterns of chromitites and associated peridotites and data scatter in the Pd/Ir versus Pt/Pt* space indicate chromitite formation by partial melting of the associated mantle rocks. The variable $^{187}Os/^{188}Os_{(i)}$ (0.1278–0.1380) and γOs (−0.38 to +7.54) values demonstrate extensive contamination of crustal components, likely in a supra-subduction zone (SSZ) setting. Combined with the occurrence of unusual 'exotic' mineral inclusions, geochemical and isotopic characteristics of the Köyceğiz chromitites replicate superimposed deep mantle processes, recycling and subduction-related phase transformations.

1. Introduction

Layered and podiform chromitites are two important sources of chromium (Cr) over the world (Shiraki, 1997). Podiform chromitites may vary from few kilograms (kg) to several millions of metric tons, and are commonly associated with mantle peridotites <500 m beneath the petrologic Moho (Zhou et al., 2005). Recent studies of ophiolites in the eastern sector of the Alpine-Himalayan mountainous chain and the Paleozoic Polar Ural orogenic belt describe micro-diamond inclusions in chromitites, suggestive of ultrahigh-pressure (UHP) conditions (e.g., Yang et al., 2014, 2015; Xiong et al., 2018a, 2019; Chen et al., 2019; Kusky et al., 2021; Kusky et al., 2022). The anticipated depth of the formation of ophiolitic chromitites varies, however, from ~8 to 30 km below the petrologic Moho (i.e., Zhou et al., 2005). Also, highly reduced minerals (e.g., moissanite (SiC), qingsongite, Fe-Si and Fe-C phases) and acicular diopside and enstatite inclusions in Cr-spinel have been reported in several ophiolitic sections of different ages (Zhou et al., 2014; Yang et al., 2014, Yang et al., 2021). The presence of these mineral phases as inclusions in Cr-spinel is considered as an indication of high-pressure precursor spinel polymorphs with orthorhombic Ca-Ferrite structure (CF; $CaFe_2O_4$) stable at P-T conditions greater than 12.5 GPa and 1400–1500 °C (Yamamoto et al., 2009). These conditions correspond to mantle depths of >380 km (Satsukawa et al., 2015). A near Mantle Transition Zone (MTZ) origin was, therefore, suggested as a part of the evolution history of some ophiolitic chromitites from different orogenic belts worldwide (e.g., Yang et al., 2007; Yamamoto et al.,

* Corresponding authors at: 26 Baiwanzhuang Street, Beijing 100037, China (F. Xiong). Department of Geology, Faculty of Science, Benha University, 13518 Benha, Egypt (B. Zoheir).
E-mail addresses: xiongfahui@126.com (F. Xiong), basem.zoheir@ifg.uni-kiel.de (B. Zoheir).

https://doi.org/10.1016/j.oregeorev.2022.104912
Received 28 December 2021; Received in revised form 16 April 2022; Accepted 20 April 2022
Available online 25 April 2022

2009; Arai, 2013; Yang et al., 2015; Satsukawa et al., 2015; Griffin et al., 2016).

Alternatively, other researchers advocate possible metastable low-pressure formation of diamond and moissanite during serpentinization of ophiolites under super-reduced conditions during or subsequent to their tectonic emplacement (e.g., Schmidt et al., 2014; Golubkova et al., 2016, Pujol-Solà et al., 2018, 2020, 2021; Machev et al., 2018; Farré-de-Pablo et al., 2019, 2020, 2021; Ballhaus et al., 2021). Golubkova et al. (2016) used thermodynamic data for alloys (Fe–Si–C and Fe–Cr), carbides (Fe_3C, Fe_7C_3, SiC), and Fe-silicides to explain moissanite occurrence in podiform chromitites by low to moderate temperature chemical isolation in the presence of ultra-reducing fluids. Pujol-Solà et al. (2018) argue against the surface lightning strikes model proposed by Ballhaus et al. al. (2017) as this model cannot explain the formation of the UHP minerals and continental inclusions in many orogenic ophiolites (e.g., Yang et al., 2007; Dobrzhinetskaya et al., 2009; Trumbull et al., 2009; Griffin et al., 2016; Yang et al., 2014, Yang et al., 2021). Similarly, some authors suggest that the oriented clinopyroxene lamellae in Cr-spinel do not necessarily indicate a high-pressure precursor, but represent minute melt inclusions trapped during continued grain growth or precipitated from late circulating fluids (e.g., Liu et al., 2020; Pujol-Solà et al., 2018; Pujol-Solà et al., 2021). Studying the available literature of twenty-five diamond-bearing ophiolites in different suture zones led Liu et al. (2021) to suggest the involvement of subcontinental lithospheric mantle in the formation of podiform chromitite. The interplay of deep mantle and post-formation crustal processes may, therefore, explain miscellaneous mineralogical and geochemical features of ophiolitic chromitites in the different orogenic belts.

As a contribution to the ongoing, yet unresolved, discussions on the origin of unusual inclusions in ophiolitic chromitites, the present study reports clinopyroxene lamellae and UHP and SuR mineral inclusions in the Köyceğiz chromitites from southwestern Turkey. Combined with the newly obtained PGE geochemical and Re-Os isotope datasets, mineralogical characteristics of these inclusions are used to assess the genesis of the Köyceğiz chromitites and associated mantle rocks. Understanding the genesis and evolution of ophiolitic chromitites provides useful information on the evolution of sub-oceanic lithospheric mantle in the western Neo-Tethys realm.

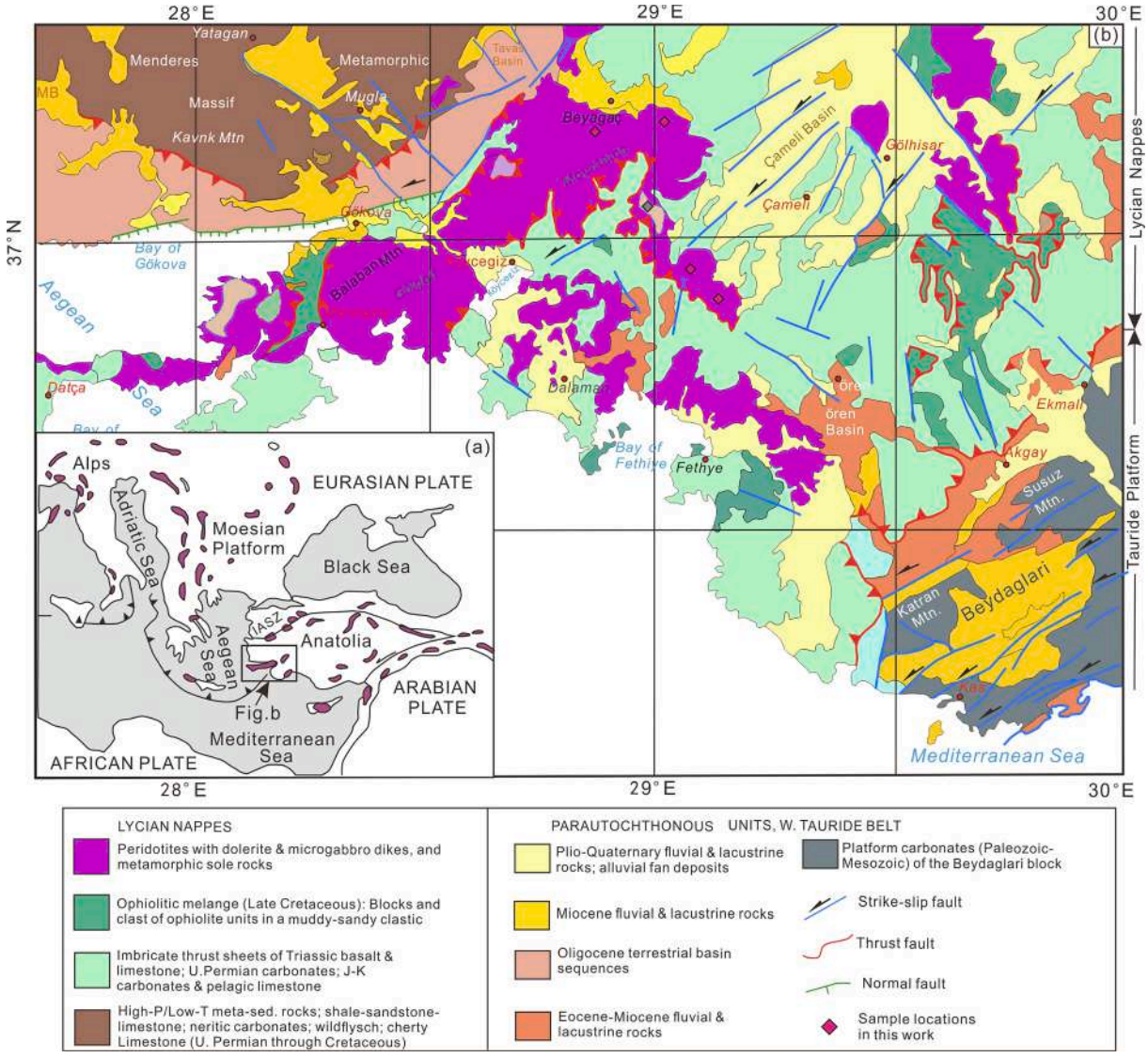

Fig. 1. (a) Simplified geological map of the Mediterranean region showing the main plate boundaries, orogenic belts, and tectonic units of Eurasian, NeoTethyan and Gondwana-Land affinities (modified from Dilek and Furnes, 2009), (b) Distribution of ophiolite units in Köyceğiz massif (modified from Okay et al., 2001). The Neotethyan ophiolites in the Eastern Mediterranean region are shown in the inset (Dilek et al., 2007). Key to abbreviations: IASZ = Izmir–Ankara Suture Zone.

2. Geological setting

2.1. Geological outline – architecture of the Köyceğiz ophiolite

In the Late Paleozoic – Early Cenozoic period, a string of continental crust fragments (known as Cimmerian micro-continents) was rifted from Gondwana, moved northward and ended to coalescence with the southern margin of Eurasia (e.g., Yin and Harrison, 2000). This process led to the closure of the Tethyan Ocean, as demonstrated by a series of discontinuous ophiolite massifs along the Alpine-Himalayan orogenic belt (Dilek et al., 2008). These ophiolites mark a system of non-linear suture zones (Fig. 1a), demarcating the original boundaries of the vanished Tethyan oceanic basins (e.g., Dilek and Furnes, 2009). Ophiolites cropping out around the eastern Mediterranean region are typical paradigms of sub-arc oceanic lithosphere and were extensively studied in the last decades (Fig. 1a; Jones and Robertson, 1991; Robertson, 2002; Rassios and Dilek, 2009; Aldanmaz, 2012; Parlak et al., 2019).

In the Western Tauride belt, extensive outcrops of mantle tectonites represent allochthonous blocks bordering a central autochthonous carbonate platform unit (Fig. 1b). According to Dilek and Rowland (1993), the Isparta Angle forms a N-trending cusp in the Tauride tectonic belt in southern Turkey. Two significant ophiolitic nappes occur around the periphery of the Isparta Angle. The Lycian nappes consist of a series of imbricate thrust sheets mainly composed of carbonate rocks (Fig. 1b). The Lycian ophiolitic massifs were thrust over the Menderes massif along a S-dipping, low-angle fault. According to Collins and Robertson (1998), the Lycian allochthon is exceptionally well-exposed and it preserves all parts of the tectonic stack and well-dated syn-tectonic sediments. Emplacement of these rocks is thought to have occurred in the Eocene, whereas transportation to the southeast over the Bey Daglari

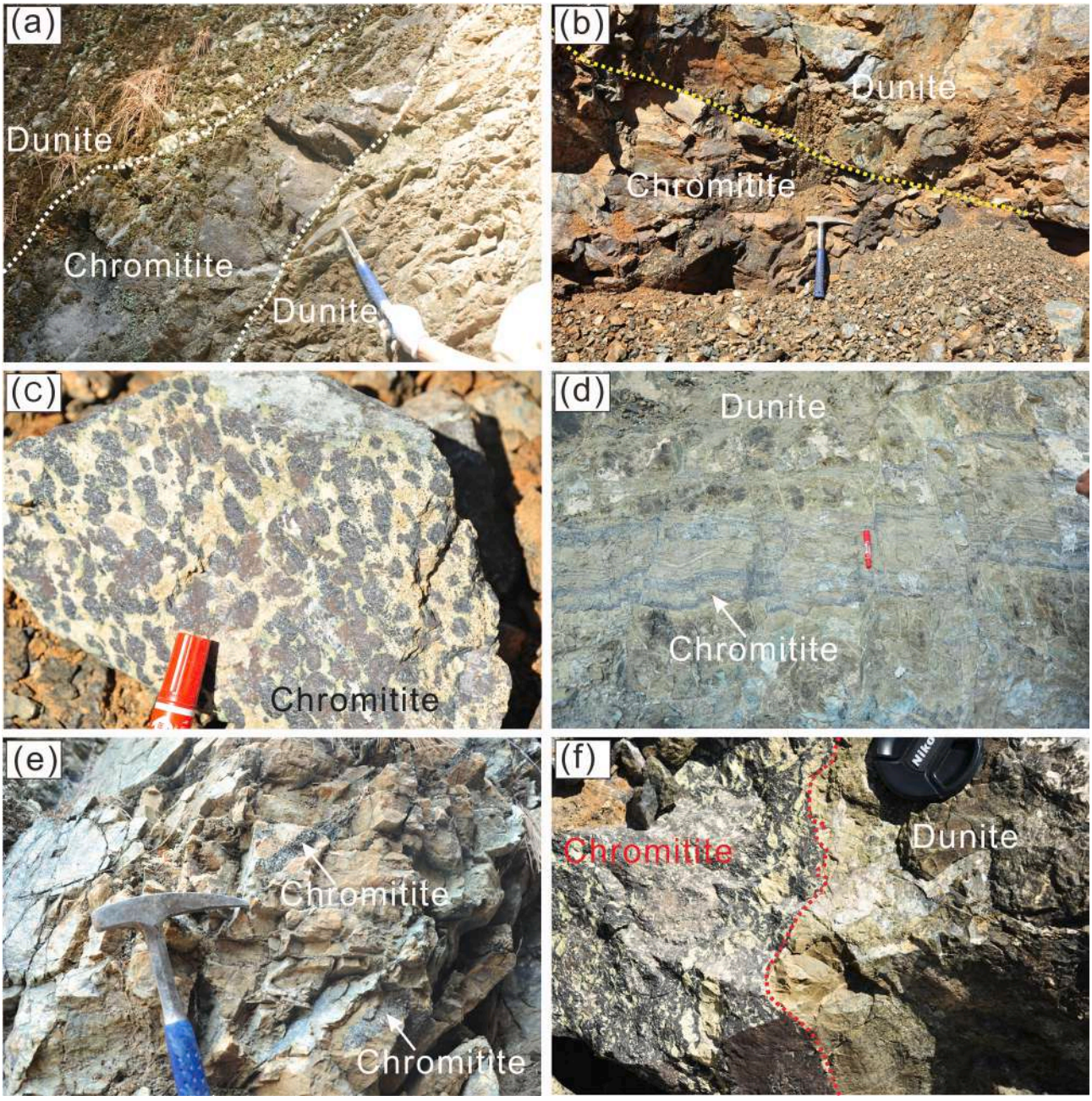

Fig. 2. Field photographs showing the different lithological units of the Köyceğiz ophiolite (a), (b) Massive chromitite lenses in dunite; (c) Nodular chromitite pods in dunite; (d) Chromitite in the Köyceğiz ophiolite; (e), (f) Chromite disseminations and thin veins in dunite.

carbonate platform occurred likely in the Miocene. The Lycian nappes contain Mesozoic-Early Tertiary continental margin-type sediments in the bottom and an upper thrust sheet of ophiolites (Robertson, 2002). Within the Lycian Thrust Sheets, rotated blocks and slickensides on fault places indicate top-to-the-southeast displacement (Collins and Robertson, 1998).

The Köyceğiz ophiolite covers an area of ~600 km^2, and is considered as one of several ultramafic massifs in the Lycian nappes. The Köyceğiz ophiolite is composed of serpentinized harzburgites, minor lherzolites, dunites and associated chromitites (Fig. 1b). Crustal volcanic and plutonic units of this ophiolitic section are generally scarce. The stratigraphy of the Köyceğiz massif is complicated by a series of thrusts. The footwall of the allochthonous massifs is an accretionary mélange of tectonically mixed marine sediments and scattered ophiolites. Amphibolite and mica schists represent sub-ophiolitic metamorphic soles underling the Lycian peridotites (Çelik and Delaloye, 2003). $^{40}Ar/^{39}Ar$ dating of amphibole and mica separates from this metamorphic sole indicates a Late Cretaceous age (~91–94 Ma) for the tectonic transport of these ophiolites (Çelik et al., 2006).

2.2. Morphological and textural characteristics of the Köyceğiz chromitites

The Köyceğiz ophiolitic chromitites occur as lenses and veins (Fig. 2a), with ore reserves measuring ~10^6 tons (e.g., Uysal et al., 2009). The ore lenses vary in thickness from 0.3 to 15 m, and extend up to ~100 m (Fig. 2a). Small chromitite lenses occur as sub-parallel <3 m-long and 20–70 cm thick bodies (Fig. 2e; Uysal et al., 2009; Xiong et al., 2018b). The chromitite lenses are locally cut by thin (10–15 cm) pyroxenite and gabbroic dykes. The vast majority of chromitite bodies exhibit sharp contacts with the enclosing dunite and harzburgite units. The Köyceğiz chromitites show various of textures, including massive (greater than 80% modal), nodular (40–80% modal), and disseminated (<40% modal) Cr-spinel ores (Fig. 2a-f). The ore bodies commonly have massive inner zones, grading to disseminated chromite in the exterior parts. Massive chromitites are mostly oriented along harzburgite foliation, showing thin (0.1–1 m) dunite envelopes. Dunite envelopes of larger thicknesses (1–5 m) commonly surround disseminated ores (Fig. 2a-f). Brittle deformation in the investigated samples is expressed by microcracks that cut across the large Cr-spinel grains (Fig. 2d).

3. Materials and methods

A set of 25 chromitite, 30 harzburgite and 16 dunite samples were collected from 20 locations in the NE part of the Köyceğiz ultramafic massif. Fifty representative polished thin sections were prepared (Supplementary Table 1). Petrographic examination of the thin sections was performed under a bi-mode transmitted and reflected light polarizing microscope. Analyses of Cr-spinel, olivine, ortho- and clinopyroxene inclusions in the Köyceğiz chromitites were performed using a JEOL JXA-8100 electron probe microanalyzer (EPMA) at the East China Institute of Technology. The analytical conditions were 15 kV accelerating voltage, 20 nA beam current, 2 μm spot diameter with a counting time of 20 s on the peaks and 10 s on the background. Calibration was done using natural and synthetic standard materials. Fe^{3+} and Fe^{2+} in Cr-spinel were calculated assuming an ideal spinel stoichiometry ($A^{2+}B_2^{3+}O_4$) following the method of Droop (1987). The results are shown in Supplementary Tables 2,3.

Concentrations of the platinum-group elements (PGE) in 10 chromitite samples, 6 harzburgite and 5 dunite samples were determined by the ICP-MS following a pre-concentration NiS fusion technique at the National Research Center of Geo-analysis (CAGS). Each sample was mixed with sodium carbonate and sodium borate, borax, glass powder, Ni and Fe powder, and S (e.g., Zhou et al., 2005). The limits of detection (in ppb) are 0.2 for Pt and Pd, 0.001 for Ir, Rh and Os, and 0.1 for Ru. The analysis precision was better than 5 % for Rh, Pd, and Ir, and 10 % for Os, Ru and Pt (Xiong et al., 2017, 2018b). Data of the bulk-rock PGE composition of chromitites and peridotites are given in Supplementary Table 4.

Re-Os isotopic measurements were carried out at the Guangzhou Institute of Geochemistry, Chinese Academy of Sciences. A quantity of 1 g to 0.6–0.7 g from each sample powder was spiked with enriched ^{190}Os and ^{185}Re solutions. The spiked samples were then digested using ca. 10 ml of inverse aqua regia (HNO_3: HCl = 3:1) in Carius tubes (Shirey and Walker, 1995) and heated up to 230 °C for 24 h. Osmium was extracted from the aqua regia fraction by the carbon tetrachloride solvent extraction technique (Cohen and Waters, 1996; Pearson and Woodland, 2000) and then back-extracted into concentrated HBr. Further purification was performed by micro-distillation with the chromic acid (Roy-Barman, 1993). Rhenium was separated and purified from the remaining aqueous solution by the anion exchange chromatography using the AG1-X8 resin (100–200 mesh).

The Re-Os isotopic ratios were determined by negative thermal ionization mass spectrometry (N-TIMS) on a Thermo-Finnigan TRITON, where Os was measured as OsO_3^- and Re as ReO_4^- (e.g., Creaser et al., 1991; Völkening et al., 1991). Osmium was loaded onto a high-purity Pt filament (99.999 %, 1 × 0.025 mm, H. Cross Co. Ltd) that had already been heated in air for more than 3 min. The Re and Os isotope compositions were measured using a static multiple Faraday collector and a pulse counting electron multiplier, respectively. The Os isotopic ratios were normalized to $^{192}Os/^{188}Os$ = 3.08271 and corrected using $^{17}O/^{16}O$ = 0.00037 and $^{18}O/^{16}O$ = 0.002047 (Nier, 1950). Rhenium isotopes were determined by the total evaporation technique (Suzuki et al., 2004). This method eliminates the instrumental mass fractionation effect, and obtains higher accuracy and precision. Duplicate measurements of the same whole-rock powder were undertaken. Detailed descriptions of the analytical procedures applied for this study are given in Suzuki and Honda (2003), Kato et al. (2005) and Li et al. (2010a), Li et al. (2010b).

Abundances of trace elements (i.e., Ti, V, Mn, Zn, Ni, Co, Ga and Sc) in Cr-spinels from 5 chromitite samples were measured by the LA-ICP-MS technique. The analyses were carried out using a 193 nm ArF excimer laser (GeoLasPro) coupled with an Agilent 7700 laser ablation (LA)-ICP-MS at the State Key Laboratory of Ore Deposit Geochemistry, institute of geology and geophysics, Chinese Academy of Sciences (CAGS). Helium (580 ml/min) was used as the carrier gas, while Ar (900 ml/min) was the make-up gas and was mixed with He via a Y-connector. The applied spot size was 44 μm, and the laser energy was 9 J/cm^2 and pulse frequency was5 Hz. Each analysis incorporated a background acquisition of approximately 30 s (gas blank) followed by 60 s of data acquisition on the unknowns. The counting time intervals for the background and unknown were 20 s and 5 s, respectively. The NIST 610 (National Institute Standards and Technology, Gaithersburg, USA) silicate glass was used as an external standard, and ^{57}Fe was selected as the internal standard. Two house standards, a komatiite glass (GOR-128) and a natural chrome (QC-Cr) were analyzed as unknowns to monitor the instrument's drift. Data reduction was completed using the online software package GLITTER (GEMOC Laser ICPMS Total Trace Element Reduction), version 4.0. The trace element compositions of Cr-spinel grains in the examined chromitites are presented in Supplementary Table 5.

A large quantity of the chromitite ore (~780 kg) was used for mineral separation at the Institute of Multipurpose Utilization of Mineral Resources (CAGS), Zhengzhou. Prior to mineral separation, the work spaces and equipment were carefully cleaned to avoid contamination. Mineral grains were recovered from each grain size class by a combination of gravity, magnetic and electrostatic techniques to obtain fragments of different sizes and densities (e.g., Xu et al., 2009). Several particles of diamond and moissanite were separated in the concentrates and were carefully picked up under a binocular and were examined using a FEI VERSA 3D scanning electron microscope (SEM) at the State Key Laboratory for Continental Tectonics and Dynamics (CAGS),

Beijing. The SEM operating conditions were 20 kV voltage and 15nA beam current.

The identification of mineral inclusions in Cr-spinels was done using a Laser Raman (RENISHAW-1000) at the State Key Laboratory for Continental Tectonics and Dynamics (CAGS). The scattered light was analyzed by a LabRam HR800 (Jobin Yvon) micro-Raman spectrometer. The spectra were acquired in the 500–1900 cm^{-1} region for diamond and the 500–1500 cm^{-1} region for moissanite, with a spectral resolution of ~ 2.0 cm^{-1}. A 50 × magnification microscope objective was used to focus light on a spot size of ~3 μm. Low laser intensities were used (~5 m W) to avoid spectral changes due to the heat-induced effects. The Raman shift was calibrated using a 520 cm^{-1} Raman band of crystalline Si. Repeated spot analyses on different diamond and moissanite grains revealed similar spectra, affirming reliable spectral reproducibility.

4. Mineral inclusions in Cr-spinel

In the Köyceğiz massif, chromitite ores consist of coarse-grained, subhedral to euhedral Cr-spinel crystals (0.5 mm to 1.2 cm). The mineral inclusions observed in Cr-spinel include olivine, orthopyroxene, clinopyroxene, hornblende, chlorite, serpentine, and apatite (Fig. 3a-c). Less abundant platinum group minerals (PGM) and sulfides were also observed in some samples (Fig. 3d). Exotic minerals, including diamond, moissanite were also scarcely reported in the studied rocks. Most of the silicate inclusions are globular in shape, and range in size from 5 to 50 μm. The euhedral inclusions show triangular and cubic habits in some cases (Fig. 3a). Some non-oriented inclusions exhibit octahedral and facets of twinning according to the crystal structure of spinels (Fig. 3g-h, j-k). Composite inclusions are typically made up of clinopyroxene and sulfide phases were also observed in some samples (Fig. 4).

Some needle-like inclusions (10–50 μm-long) show a preferential

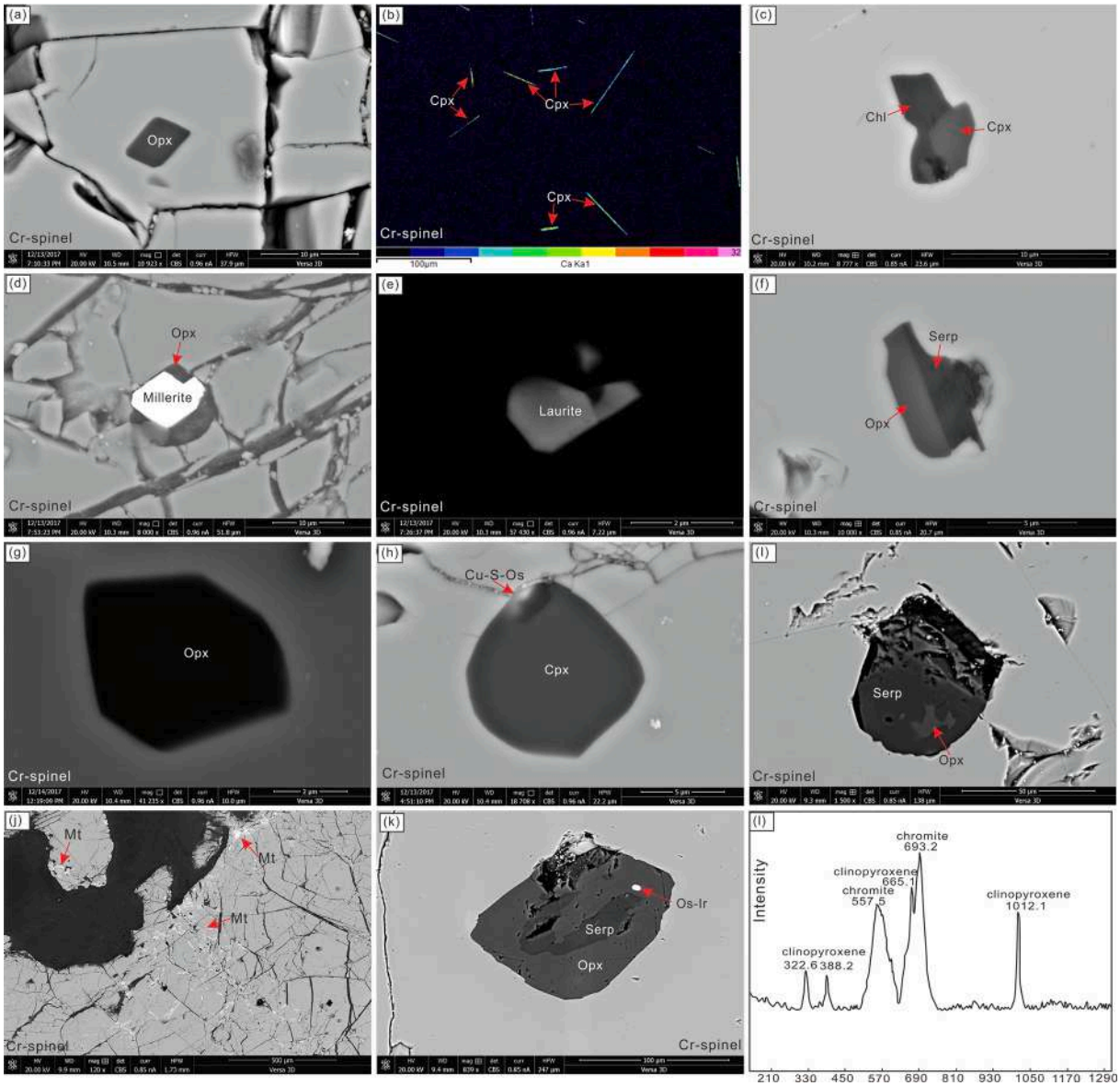

Fig. 3. BSE images of inclusions in the Cr-spinel grains from the Köyceğiz chromitites; (a) Orthopyroxene; (b) Lamellar/needle-shaped silicate micro-inclusions with Ca element mapping; (c) Cpx and chlorite as inclusions in Cr-spinel; (d) Millerite with opx; (e) Laurite; (f) Orthopyroxene with serpentine; (g) Randomly distributed globular/anhedral opx inclusions in the magnesiochromites; (h) Randomly distributed globular/anhedral opx intergrown with Cu-S-Os phase inclusions; (i) Orthopyroxene with serpentine; (j) Some parts of Cr-spinel with magnetization; (k) Orthopyroxene with serpentine; In (l), Raman spectra of some of the relatively larger lamellar/needle-shaped micro inclusions within Cr-spinelhosts of the Köyceğiz chromitites. Cpx: clinopyroxene; Opx: orthopyroxene; Cr-spinel: chromian spinel; Mt: Magnetite.

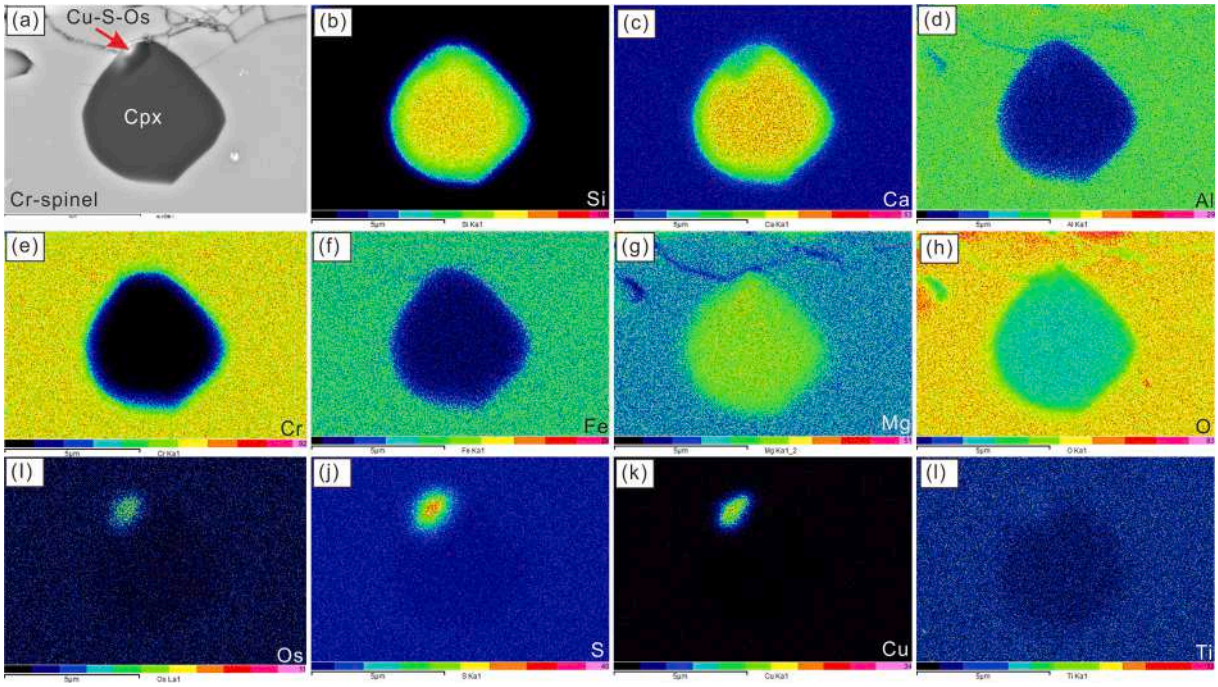

Fig. 4. (a) to (i) BSE images and X-Ray elemental maps of globular/anhedral Cpx and a Cu-Os sulfide in the Cr-spl.

distribution along the (1 1 1) crystallographic planes in the host Cr-spinel grains (Fig. 5a). The X-ray elemental mapping shows that these inclusions are rich in Si, Ca and Mg (Fig. 5b, c, e), and devoid Cr, Al, and Fe (Fig. 5f, g, h). The energy-dispersive (ED) and wavelength-dispersive (WDS) spectroscopic analyses of the large needles indicate a diopside composition. In addition, repeated Raman analyses gave spectra with characteristic bands at 322.6, 388.2, 665.1 and 1012.1 cm^{-1}. These peaks correspond to the M–O stretching (~327 cm^{-1}), Mg-O stretching (~393 cm^{-1}), Si-O-Si bending (~665 cm^{-1}), and Si-$O^{(br)}$ stretching (~1010 cm^{-1}) modes of diopside (Fig. 3l, Huang et al., 2000). The Raman shifts for the silicate micro-inclusions are expected to deviate somewhat from pure diopside due to the spurious fluorescence effect by the host Cr-spinel. The reported raman peaks found at 557.2 and 693.2 cm^{-1} (Fig. 3l) can be related to the $F_{2g(2)}$ and A_{1g} modes of Cr-bearing spinel (Lenaz and Lughi, 2013, 2017; D'Ippolito et al., 2015).

In addition to the silicate and sulfide inclusions, about 25 subhedral diamond fragments were recovered from the Köyceğiz chromitites. Most of these microdiamonds are pale yellow to light green (Fig. 6a) and range in size from 50 to 200 μm (Fig. 6a). They are free of mineral inclusions, micro-pores and overgrowths. Raman shifts of these micro-diamonds are all around 1332 cm^{-1} (Fig. 6c) and their full widths at half maximum (FWHM) are at 1330–1332 cm^{-1}. These characteristics are similar to the micro-diamonds reported in the Luobusa ophiolite (Xu et al., 2009), and are clearly distinct from the metamorphic diamonds (Korsakov et al., 2005). Forty moissanite grains were separated from the Köyceğiz chromitites. They are anhedral, transparent, light to dark blue (30 to 280 μm-large) grains (Fig. 6b), and yield Raman peaks at 762 cm^{-1}, 785 cm^{-1} and 966 cm^{-1} shifts (Fig. 6d). Moissanite grains with comparable morphologies and spectral characteristics were separated from chromitites from the Pozanti-Karsanti ophiolitic massif in Turkey (Lian et al., 2017).

5. Geochemical characteristics of the Köyceğiz chromitites

5.1. Cr-spinel composition

The Cr-spinel grains from the investigated Köyceğiz chromitite samples have concentrations of Al_2O_3 (9.87–10.69 wt%), Cr_2O_3 (55.14–56.95 wt%), FeO^t (16.51–18.13 wt%) and MgO (14.13–15.13 wt %), typical of the ophiolitic chromitites (e.g., Bonavia et al., 1993; González-Jiménez et al., 2014; Supplementary Table 2). The analyzed Cr-spinel grains have Cr# [Cr/(Cr + Al) × 100] ranging from 78 to 79, and Mg# [Mg/(Mg + Fe^{2+}) × 100] values of 61–77, classifying the Köyceğiz as high-Cr or metallurgical-type chromitites (Leblanc and Nicolas, 1992). Further, the abundances of many trace elements in Cr-spinel from the Köyceğiz chromitites are generally low (Supplementary Table 2), which is typical of high-Cr ophiolitic chromitites (e.g., Bonavia et al., 1993). In the Al_2O_3 vs. TiO_2 discrimination diagram (Dick and Bullen, 1984; Barnes and Roeder, 2001; Kamenetsky et al., 2001), Cr-spinel data of the Köyceğiz ores resemble spinels in equilibrium with boninitic melts (Fig. 7).

The concentrations of several trace elements, i.e., Ti, Ni, V, Mn, Zn, Sc, Co and Ga, by LA-ICP-MS were determined for unaltered cores of the large Cr-spinel grains. No considerable variations in the trace element abundances were observed among the different chromitite samples. Limited variations were only reported for Ni (932–1104 ppm), V (540 – 586 ppm), Zn (246 – 342 ppm), Co (180 – 198 ppm), Ga (16.4 – 20 ppm) and Sc (6 – 10 ppm) (Supplementary Table 5). If normalized to the composition of Cr-spinels from the East Pacific Rise MORB (Chr^{MORB}), the Köyceğiz chromitites are characterized by a mild positive Ti anomaly and a weak negative V anomaly (Fig. 8). Their trace element patterns are similar to Cr-spinel from boninites and high-Cr chromitites of the Thetford Mines ophiolite (TMO) in Québec (Pagé and Barnes, 2009).

5.2. Chemical characteristics of the mineral inclusions

In the Cr-Spinel grains, orthopyroxene inclusions are mostly enstatite in composition (95.7–96.3%; Fig. 9a), with Cr_2O_3 and Al_2O_3 contents of 0.79 to 1.13 wt% and 0.37 to 0.47 wt%, respectively. The TiO_2 contents are generally low (≤0.09 wt%; Supplementary Table 3). Clinopyroxene inclusions have a diopside composition, with less variable Wo and En contents of 45.8–48.1 wt% and 50.7–52.5 wt%, respectively (Fig. 9a). The Al_2O_3 contents range from 0.50 to 0.76 wt% and Na_2O contents are between 0.16 and 0.20 wt%; Supplementary Table 3). The calculated Mg# values are generally high for orthopyroxene (96.4–96.8) and clinopyroxene (96.9–97.7) inclusions (Supplementary Table 3). Olivine

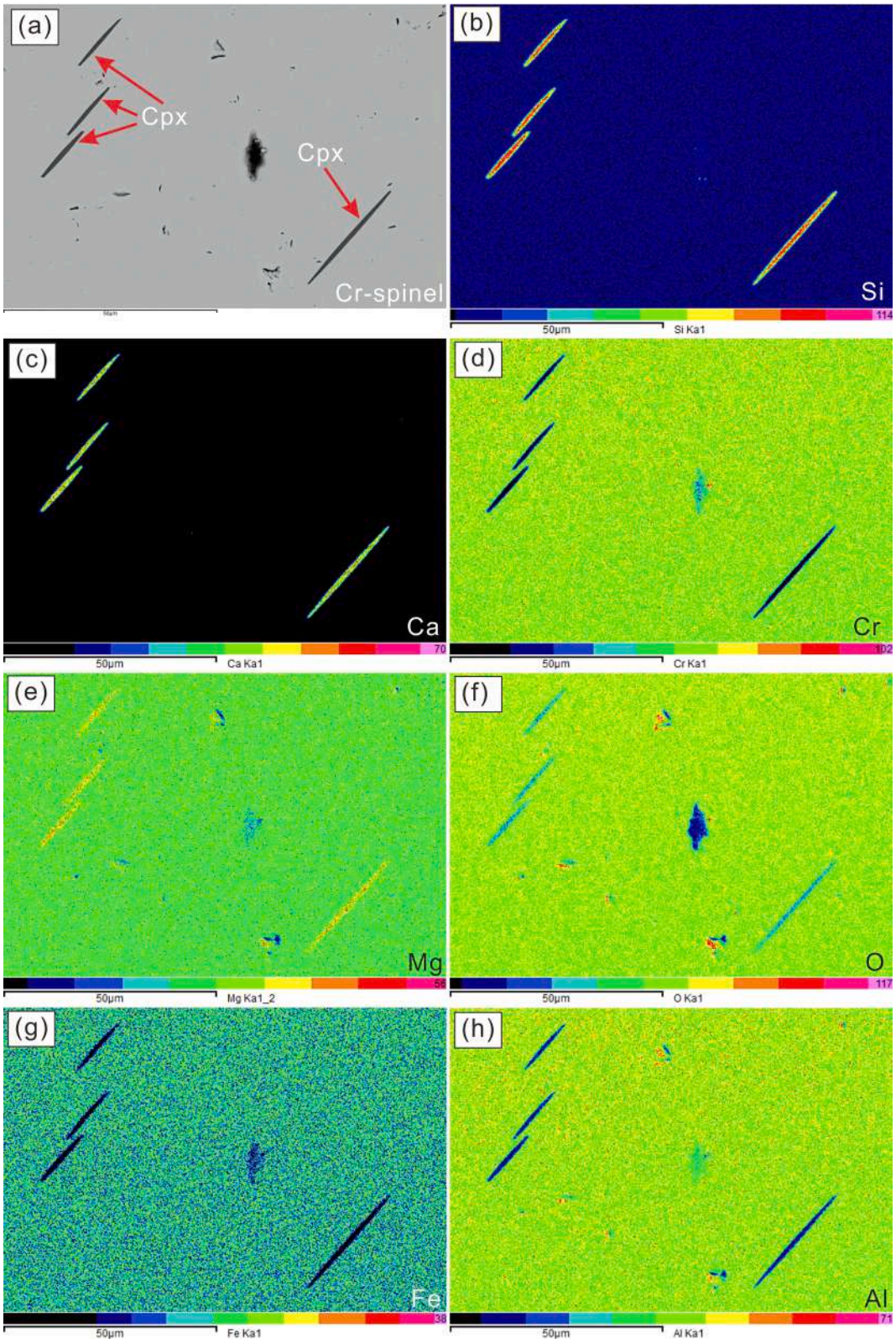

Fig. 5. (a) to (h) BSE images and X-Ray elemental maps of lamellar/needle-shaped silicate micro-inclusion from Köyceğiz chromitites.

inclusions are characterized by high Fo (97.9–98.26) and high NiO contents (1.11–1.18 wt%; Fig. 9b), whereas the MnO contents are invariably below the EPMA detection limit; Supplementary Table 3).

5.3. Platinum group element (PGE) composition

Dunites and harzburgites from the Köyceğiz ophiolite have similar PGE abundances, with ΣPGE concentrations between 10.13 and 63.88 ppb, and Pd/Ir = 0.15–2.15 (Supplementary Table 4). The bulk-rock

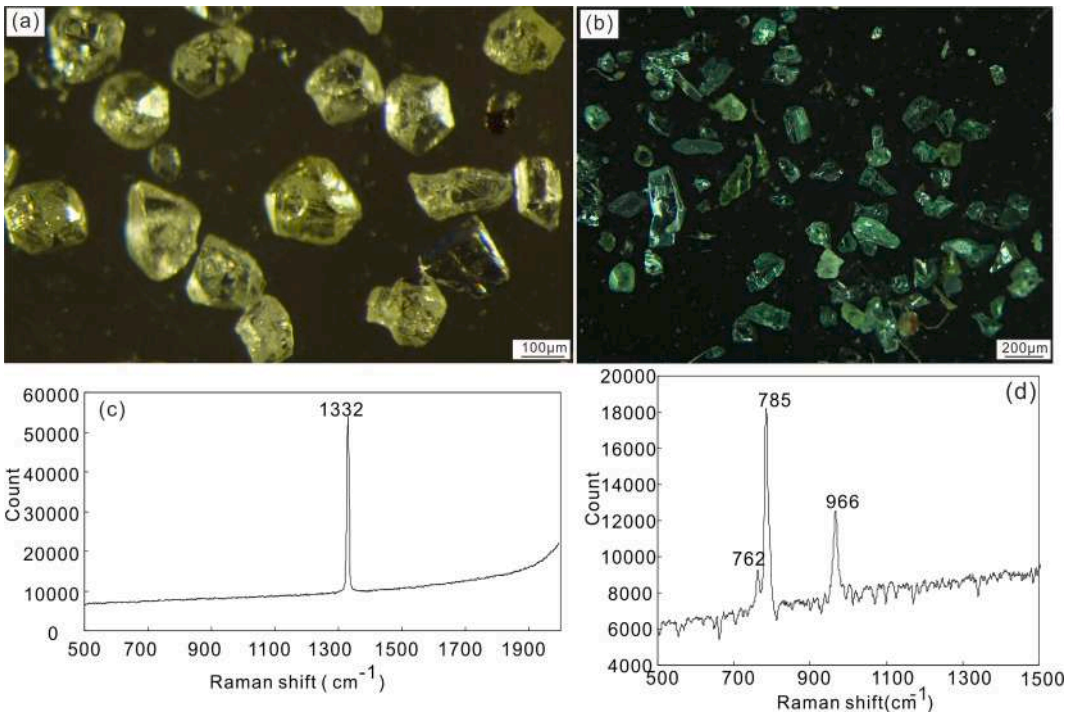

Fig.6. Microphotographs and Raman spectra of microdiamonds and moissanites separated from the Köyceğiz chromitite. (a) Microdiamonds showing their color and morphology; (b) Moissanite grains with their color range and fragmented; (c) Raman spectra of microdiamonds; (d) Raman spectra of Moissanite.

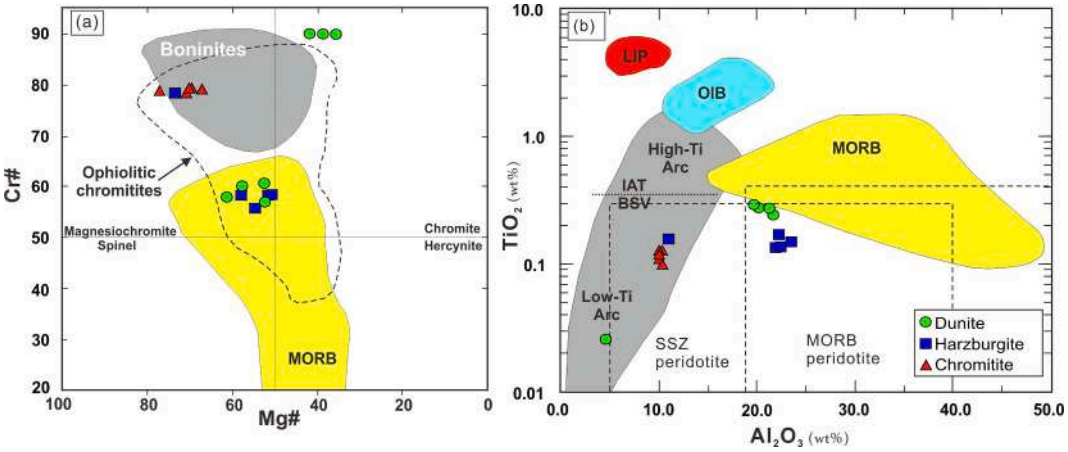

Fig. 7. (a) Cr# [Cr/(Cr + Al) × 100] vs. Mg# [Mg/(Mg + Fe^{2+}) × 100] plot of Cr-spinel from the Köyceğiz chromitites. Fields for spinel in equilibrium with N-MORBs and boninites are from Dick and Bullen (1984). (b) TiO_2 vs. Al_2O_3 diagram. Compositional fields are from Kamenetsky et al. (2001). Abbreviations: BSV: boninite series volcanics, IAT: island arc tholeiites, MORB: mid-ocean ridge basalts, OIB: Ocean Island Basalts, LIP: Large Igneous Province.

PGE concentrations in the Köyceğiz chromitites range from 80 to 442 ppb (Supplementary Table 4), within the typical range of ophiolitic chromitites (144–1064 ppb; Najafzadeh and Ahmadipour, 2014). The large variations in the PGE abundances suggest heterogeneous distributions of these elements in the studied rocks, and perhaps related to scattered IPGM inclusions (i.e., laurite; Fig. 3d). The Köyceğiz chromitites show enrichments in the iridium-group PGE (IPGE: Os, Ir and Ru; 76–427 ppb) relative to the palladium-group PGE (PPGE: Rh, Pt and Pd; 4–15 ppb). All analyzed samples have small Pd/Ir (≤0.09) and PPGE/IPGE (0.03–0.06) values.

The primitive mantle-normalized PGE patterns of the Köyceğiz chromitites are characterized by a gentle negative slope from Os to Rh and a steep slope between Rh-Pd. Some samples, however, show positive slopes between Pt and Pd (Fig. 10b). These patterns are comparable to those of other high-Cr chromitites in south Turkey (e.g., Uysal et al., 2016; Fig. 10b).

5.4. Re-Os isotope systematics

Six chromitite samples have been analyzed for their Re and Os isotopic composition (Supplementary Table 6). The abundances of Os and Re are 27.1–305.8 ppb and 0.09–0.18 ppb, respectively. The $^{187}Os/^{188}Os$ ratios (0.12781–0.13798) are consistently larger than the present-day chondritic value (0.1275; Walker et al., 1989) and are mostly greater than the primitive mantle value (0.1296; Meisel et al., 2001) (Fig. 11). The calculated $^{187}Os/^{188}Os_{(i)}$ ratios are 0.1278–0.1380 ($\gamma Os = -0.38$ to $+7.54$), similar to other Neo-Tethys podiform chromitites and peridotites in the eastern Mediterranean region (Lapierre et al., 2004). Most of the samples yielded γOs values larger than the PM value, implying variable contamination of crustal components. The

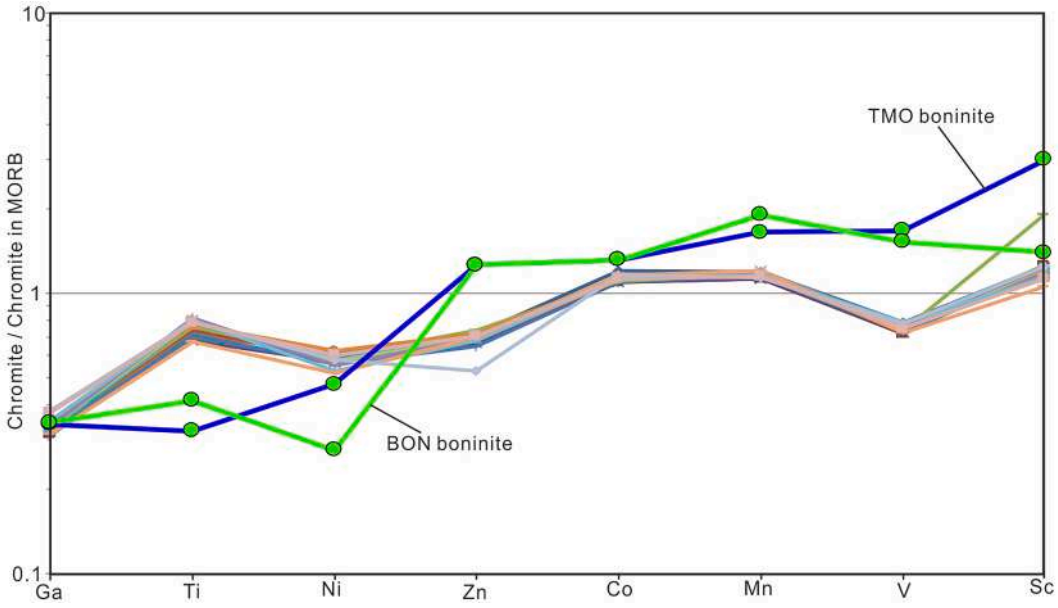

Fig. 8. MORB-normalized trace element patterns of parental magmas for the Köyceğiz chromitite (Pagé and Barnes, 2009). BON: boninite from Bonin Island; TMO: boninite from the Thetford Mines Ophiolite (Pagé and Barnes, 2009).

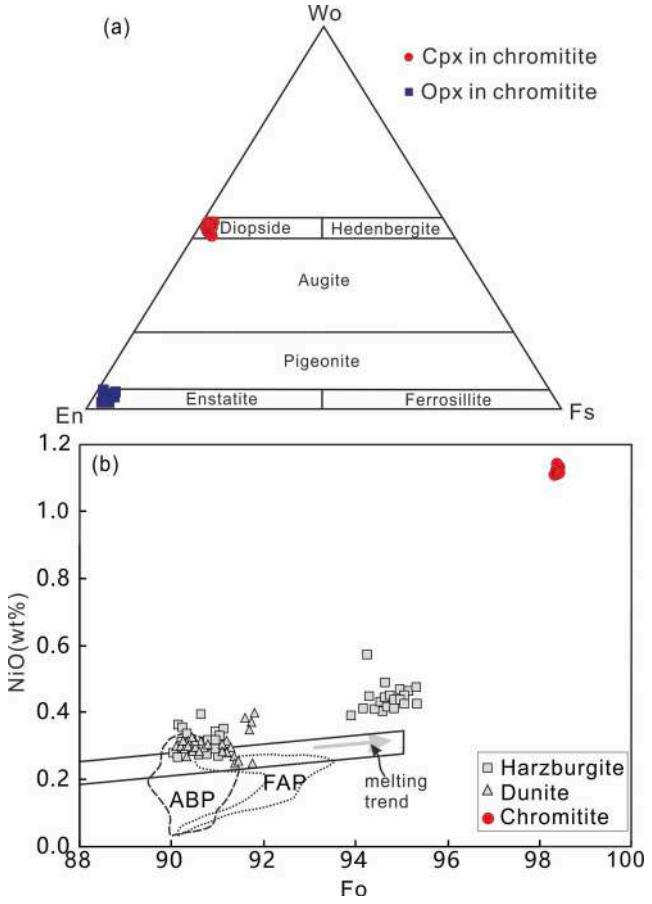

Fig. 9. Compositional variations of silicate inclusion in the studied chromitites. (a) Pyroxene quadrilateral for ortho- and clinopyroxene; (b) Olivine NiO vs. Forsterite (Fo) compositional diagram for the different lithologies of the Köyceğiz chromitites and peridotites; the mantle olivine array is from Takahashi (1986), partial melting trends are from Ozawa (1994) and Nakamura (1995). ABP: abyssal peridotites; FAP: = fore-arc peridotites (from Pagé et al., 2008).

studied chromitite samples have $^{187}Re/^{188}Os$ ratios of 0.0019–0.0213, which are inferior than the PUM value (~0.40; Meisel et al., 2001).

6. Discussion

6.1. Geochemical and isotopic characteristics of the Köyceğiz chromitites

Podiform chromitites may form at both oceanic and arc-related settings, and is commonly attributed to the interaction of mantle harzburgite with subduction-related hydrous melts (e.g., Zhou et al., 2005; Gonzalez-Jimenez et al., 2011; Xiong et al., 2018a, b). The absolute abundances and normalized patterns of PGE in chromitites are crucial tools in assessing the petrological processes operating in the upper mantle, e.g., partial melting, melt extraction, and melt percolation (Zhou et al., 2005; Prichard et al., 2008; Su et al., 2015, 2020).

Previous studies indicate that SSZ ophiolitic chromitites can preserve positive IPGE (Ir and Ru) ± Rh anomalies and negative-slope primitive mantle-normalized patterns (e.g., Lay et al., 2017; Xiong et al., 2018b). These anomalies are explained by Os and Ir are compatible elements in Cr-spinel, whereas Pt and Pd are strongly incompatible elements. The melting of residual mantle peridotite in subduction zones produces boninitic magma, and the reaction of rock melt occurs, making the magma strongly unsaturated in sulfur, relatively enriched in PGE, especially IPGE, which supports high Cr-type chromite formation from a boninitic magma (Hickey and Frey, 1982; Zhou et al., 1998).

The Cr# values in dunites, harzburgites, and high-Cr chromitites are generally greater than 60, suggesting a subduction-related processes for the genesis of the Köyceğiz ophiolite (Fig. 7). The Köyceğiz high-Cr chromitites were most likely derived from melts produced by heterogeneous melting of a SSZ mantle column (Fig. 7; e.g., Uysal et al., 2005, 2007, 2012, 2018; Xiong et al., 2018b; Ning et al., 2020; Huang et al., 2021). The Köyceğiz chromitites are enriched in IPGE (Ir and Ru) ± Rh relative to PPGE contents. The lack of covariance of Pt/Pt* [$Pt_N/(Rh_N \times Pd_N)^{1/2}$] and Pd/Ir (Fig. 12) suggests that the PGE contents in these chromitites were controlled by differentiation of the parental magma (Fig. 10).

Fig. 10 shows the PGE patterns of chromitites, notably distinct from those of the associated peridotites. Harzburgite data arrayed flat primitive mantle-normalized patterns with negative Pt anomalies (Fig. 10a). Dunite samples show patterns similar to those of the harzburgite

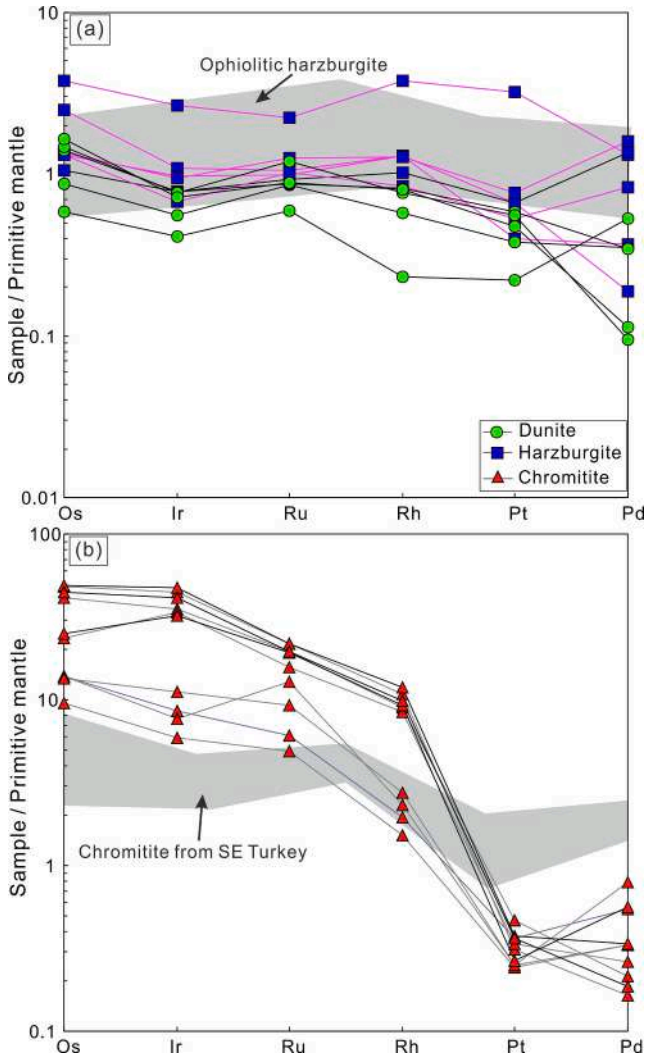

Fig. 10. Primitive mantle (PM)-normalized patterns (Barnes et al., 1985) of the Köyceğiz (a) peridotites and (b) chromitites and their comparison with those from the mantle-hosted chromitites of high-Al chromitite from southeastern Turkey (Akmaz et al., 2014), Herbeira (Moreno et al., 2001) and Thetford Mines ophiolite (Gauthier et al., 1990) as well as PGE values of average mantle (Sun and Sun, 2005) are used here for comparison.

samples, except for the relative depletions in Pt and Pd contents. Chromitites, on the other hand, are generally enriched in the PGE compared to harzburgite and dunite samples. The PGE pattern of Köyceğiz chromitites, if compared with the associated peridotites, indicate significant enrichment of IPGE (Fig. 10). These distinctive PGE patterns may imply a heterogeneous melting genesis and/or reflect variable conditions during the formation of the Köyceğiz ophiolites (Uysal et al., 2012). The Köyceğiz chromitites have Re concentrations similar to those of the associated peridotites, but higher Os contents (Fig. 11), likely related to dispersed Os-bearing inclusions or superimposing magmatic increments.

The podiform chromitites have highly variable $^{187}Os/^{188}Os$ values, as a result of processes including contamination of radiogenic Os by recycling of oceanic crust, metasomatism, and melt-fluid percolation into mantle peridotites (e.g., Alard et al., 2002; Büchl et al., 2004; Reisberg et al., 2004; Shi et al., 2007; Marchesi et al., 2011). Walker et al. (2002) determined a well-defined average $^{187}Os/^{188}Os$ value of 0.12809 and concluded that dehydration of the oceanic crust in subduction zones has no significant effect on the Os isotope composition of ophiolitic chromitites. Variations in the $^{187}Os/^{188}Os$ and γOs values for the studied chromitites and associated peridotites may therefore reflect different parental magmas (Uysal et al., 2012). According to Rudnick and Walker (2009), reaction of ~20% basaltic melt with mantle peridotites does not cause significant change in the $^{187}Os/^{188}Os$ ratio. The highly radiogenic $^{187}Os/^{188}Os$ values in the examined ophiolites can therefore represent signs of recycled radiogenic Os in the mantle wedges (e.g., Xiong and Wood, 1999; McInnes et al., 1999; Widom et al., 2003).

The evolution of the Köyceğiz peridotites could have commenced in an intraoceanic subduction zone, where radiogenic Os-enriched lithosphere occurred beneath a section of hitherto depleted peridotites (cf., Bradon et al., 1996). As incongruent melting increased, pyroxene was partially or completely removed and the interstitial MgO-rich olivine high-Cr spinel were added (Zhou et al., 2005). Similar to other ophiolites along the Indus-Yarlung Zangbo suture, the Köyceğiz ophiolites could have formed in a MOR setting and were then modified in a SSZ environment (Xu et al., 2011; Yang et al., 2011; Xiong et al., 2015a, b; Liu et al., 2014; Zhou et al., 2019).

6.2. *Formation and exhumation of the UHP Köyceğiz chromitites*

Typical characteristics of the UHP ophiolitic chromitites include: i) occurrence of spherical inclusions of Fe-Ti alloy and nano-phases of TiO_2 (Dobrzhinetskaya et al., 2009; Xiong et al., 2022a, b); ii) Cr-spinel with abundant native Fe spherules which suggest original high-pressure Ca-ferrite structured Cr-spinel polymorph (McGowan et al., 2015); iii) needles of SiO_2 (i.e., coesite), diopside, and rarely enstatite with preferred crystallographic orientations (Yamamoto et al., 2009); iv) cubic Mg-silicate with Si in octahedral coordination, and antigorite pseudomorphs in Cr-spinel as evidence of subduction-related dehydration under ringwoodite-wadsleyite stability fields (Bindi et al., 2018); and v) coarse symplectitic intergrowths of orthopyroxene + spinel ± clinopyroxene interpreted as breakdown products of high-P majoritic garnets (e.g., Morishita and Arai, 2003; Tubía et al., 2004; Piccardo et al., 2007; Xiong et al., 2015a).

The micro-diamonds, moissanite, and lamellar diopside inclusions in the Köyceğiz chromitites may suggest UHP deep-mantle recycling as the mechanism of formation of these rocks (Figs. 5, 6; e.g., Yamamoto et al., 2009; Satsukawa et al., 2015; Griffin et al., 2016; Xiong et al., 2021; Rui et al., 2022). Clinopyroxene exsolutions in low-P Cr-spinel may represent pseudomorphs of former hydrous mineral inclusions in Cr-spinel formed as a result of decompression of high-P mantle region in shallower mantle levels (e.g., Yamamoto et al., 2009). No coesite inclusions have been observed in the investigated chromitite samples, which may indicate that the pressure variation-induced inversion of spinel pseudomorphs during recycling may have been incomplete (Yamamoto et al., 2009).

A genetic model or scenario of the formation and evolution of the Köyceğiz chromitites may include: (i) early crystallization of chromitite from boninitic melts derived from a hydrated mantle wedge above a subducting slab and during peridotite-melt reaction (e.g., Robertson, 2002; Uysal et al., 2007; Xiong et al., 2018a), (ii) clinopyroxene exsolutions in the Cr-spinel by pressure variations during mantle convection and upwelling to shallower levels (Yang et al., 2007, Yang et al., 2015), (iii) transformation of Cr-spinel to high-P spinel polymorphs and hydrous mineral inclusions disappear. Moissanite may have formed as a result of C-rich subduction-related fluids in the SSZ setting (e.g., Trumbull et al., 2009), (iv) the subducting slabs migrated back into the mantle, while some portions were entrapped as SSZ mantle (e.g., Dilek et al., 2008). Extensive serpentinization, as indicated by abundant serpentine inclusions in well-preserved Cr-spinel grains, could have occurred in the subduction environment instead of post-emplacement alteration.

Juteau et al. (1977) suggested that mantle lineations radiating away from a central point in the Antalya ophiolite of southern Turkey may reflect evidence of mantle rose in diapiric form. The antiformal structures that characterize the Tauride ophiolites may reflect variations in

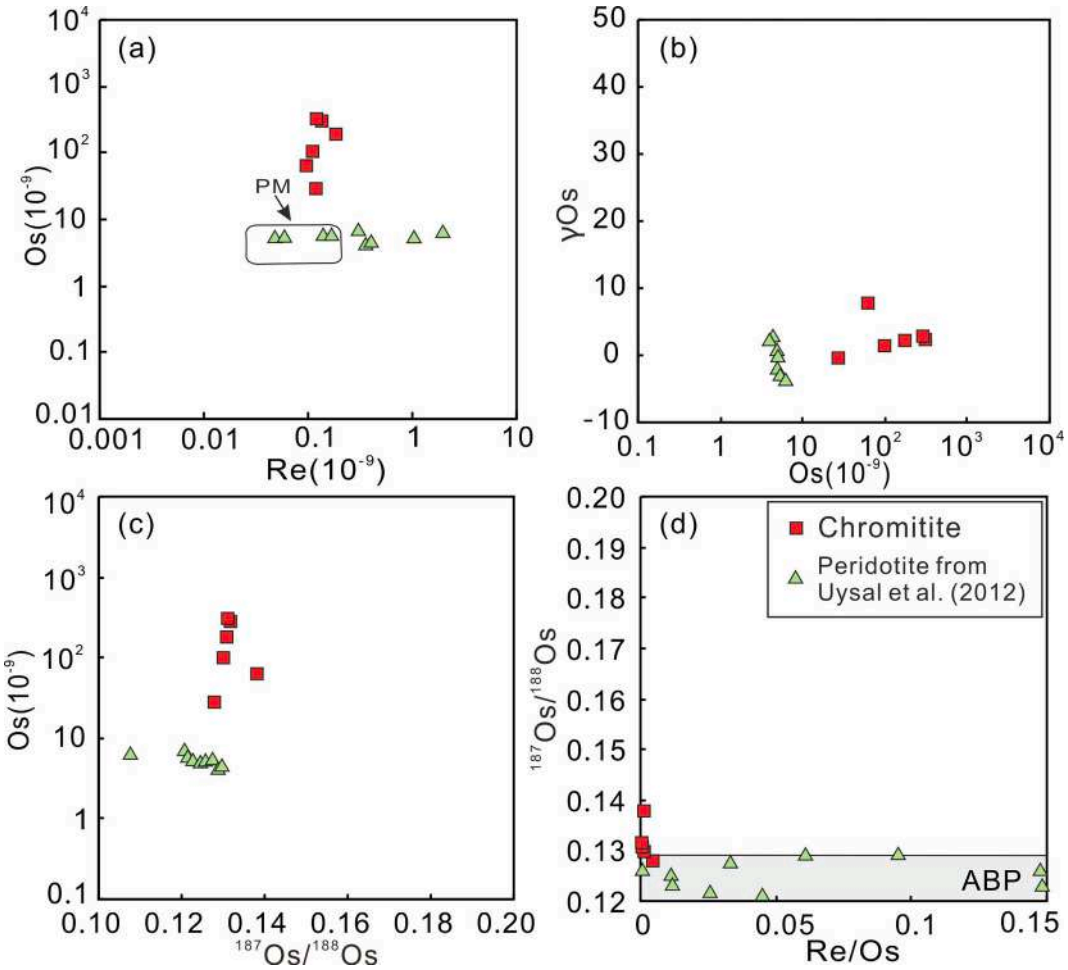

Fig. 11. The Re-Os compositions and isotopic characteristics of Köyceğiz ophiolitic peridotites and chromitites. The peridotites data are from Uysal et al. (2009). ABP: abyssal peridotite, PUM: primitive mantle. Data for primitive mantle from Meisel et al (2001), and data for the abyssal peridotites from Brandon et al. (2000), Harvey et al. (2006) and Liu et al. (2008).

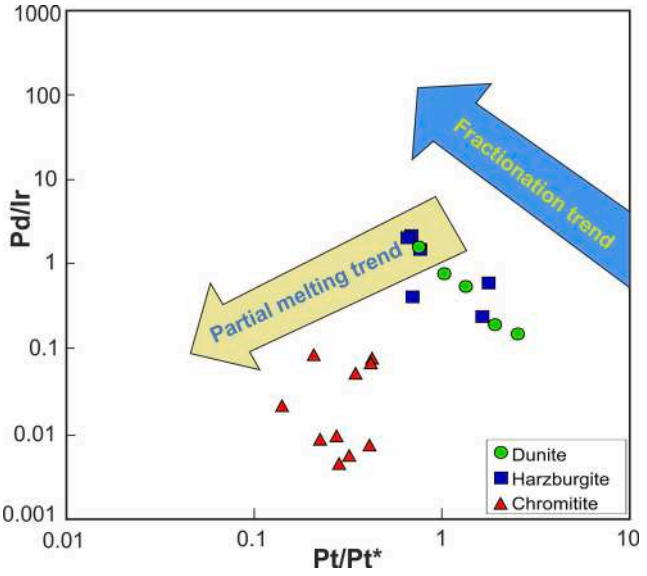

Fig. 12. Pd/Ir vs. Pt/Pt* diagram for the Köyceğiz ophiolite. Average composition of the asthenosphere as well as fractionation and partial melting trends are from Garuti et al. (1997). The platinum (Pt) anomaly is calculated as follows: $Pt/Pt^* = (Pt/8.3)/[(Rh/l.6) \times (Pd/4.4)]^{1/2}$.

the intensity and nature of primary deformation as surges of asthenospheric mantle moved at different rates and depths away from diapiric centres (e.g., Bartholomew, 1993). Diapiric upwelling could also be anticipated for the formation of the Köyceğiz ophiolites considering the presence of exotic UHP and SuR mineral inclusions and variable PGE signatures of chromitites and the associated peridotites.

7. Conclusions

Field relationships and microtextural characteristics, integrated with new bulk-rock geochemical and PGE data of the Köyceğiz chromitites support deep mantle, recycling, subduction zone and syn- to post-emplacement processes. Chromitite nodules with dunite and widespread impregnation textures, together with fractionated PGE patterns and radiogenic Re-Os data, accentuate the supra-subduction zone (SSZ) environment.

Formation of the Köyceğiz was related to wet melting of mantle peridotites and extensive contamination of crustal components. The unusual mineral inclusions in Cr-spinel grains coupled with heterogeneous geochemical and isotopic characteristics of the Köyceğiz chromitites replicate superimposed UHP and SuR deep mantle conditions, recycling and subduction-related phase transformations. Despite the yet unconstrained mode of ophiolite emplacement, widespread antiformal structures and thrusts associated the allochthonous Tauride ophiolites may demonstrate possible trans-lithospheric diapiric recycling in the region during the Late Cretaceous. This study concludes

that deep upper mantle processes and subduction-related processes may have interplayed during the formation of important high-Cr chromitite ores.

Declaration of Competing Interest

The authors declare that they have no known competing financial interests or personal relationships that could have appeared to influence the work reported in this paper.

Acknowledgements

We are indebted to Yildirim Dilek, Ibrahim Uysal and Dr. Dongyang Lian for their help during the fieldwork. This research was made possible through financial support from the National Natural Science Foundation of China (NNSFC; Project No. 92062215, 41720104009, 42172069), the Second Tibetan Plateau Scientific Expedition and Research Program (No. 2019QZKK0801), Key Special Project for Introduced Talents Team of Southern Marine Science and Engineering Guangdong Laboratory (Guangzhou) (No. GML2019ZD0201), the Key Laboratory of Deep-Earth Dynamics of Ministry of Natural Resources Fund (No. J1901-28, J1901-3), and the China Geological Survey (CGS; Project Nos. DD20221817, DD20221657). Basem Zoheir likes to acknowledge the Alexander von Humboldt Foundation for supporting his research stay at Kiel. Ibrahim Uysal (AE) and two anonymous reviewers are thanked for the professional editorial handling, through reviews, and for many insightful suggestions to improve an early version of this paper.

Appendix A. Supplementary data

Supplementary data to this article can be found online at https://doi.org/10.1016/j.oregeorev.2022.104912.

References

Akmaz, R.M., Uysal, I., Saka, S., 2014. Compositional variations of chromitite and solid inclusions in ophiolitic chromitites from the southeastern Turkey: implications for chromitite genesis. Ore Geol. Rev. 58, 208–224. https://doi.org/10.1016/j.oregeorev.2013.11.007.

Alard, O., Griffin, W.L., Pearson, N.J., Lorand, J.-P., O'Reilly, S.Y., 2002. New insights into the Re–Os systematics of sub-continental lithospheric mantle from in situ analysis of sulphides. Earth Planet. Sci. Lett. 203 (2), 651–663. https://doi.org/10.1016/S0012-821X(02)00799-9.

Aldanmaz, E., 2012. Trace element geochemistry of primary mantle minerals in spinel peridotites from polygenetic MOR-SSZ suites of SW Turkey: constraints from an LA-ICP-MS study and implications for mantle metasomatism. Geol. J. 47 (1), 59–76. https://doi.org/10.1002/gj.v47.110.1002/gj.1336.

Arai, S., 2013. Conversion of low-pressure chromitites to ultrahigh-pressure chromitites by deep recycling: a good inference. Earth Planet. Sci. Lett. 379, 81–87. https://doi.org/10.1016/j.epsl.2013.08.006.

Ballhaus, C., Helmy, H.M., Fonseca, R.O.C., Wirth, R., Schreiber, A., Jöns, N., 2021. Ultra-reduced phases in ophiolites cannot come from Earth's mantle. Am. Mineral. 106 (7), 1053–1063. https://doi.org/10.2138/am-2021-7612.

Barnes, S.J., Roeder, P.L., 2001. The range of spinel compositions in terrestrial mafic and ultramafic rocks. J. Petrol. 42, 2279–2302. https://doi.org/10.1093/petrology/42.12.2279.

Bartholomew, I.D., 1993. The interaction and geometries of diapiric uprise centres along mid-ocean ridges – evidence from mantle fabric studies of ophiolite complexes. Geol. Soc. 76 (1), 245–256. https://doi.org/10.1144/gsl.sp.1993.076.01.11.

Bindi, L., Griffin, W.L., Panero, W.R., Sirotkina, E., Bobrov, A., Irifune, T., 2018. Synthesis of inverse ringwoodite sheds light on the subduction history of Tibetan ophiolites. Sci. Rep. 8, 5457. https://doi.org/10.1038/s41598-018-23790-9.

Bonavia, F.F., Diella, V., Ferrario, A., 1993. Precambrian podiform chromitites from Kenticha Hill, Southern Ethiopia. Econ. Geol. 88, 198–202. https://doi.org/10.2113/gsecongeo.88.1.198.

Büchl, A., Brügmann, G.E., Batanova, V.G., Hofmann, A.W., 2004. Os mobilization during melt percolation: the evolution of Os isotope heterogeneities in the mantle sequence of the Troodos ophiolite, Cyprus. Geochim. Cosmochim. Acta 68 (16), 3397–3408. https://doi.org/10.1016/j.gca.2004.02.005.

Çelik, Ö.F., Delaloye, M., 2003. Origin of metamorphic soles and their post-inematic mafic dyke swarms in the Antalya and Lycian ophiolites, SW Turkey. Geol. J. 38, 235–256. https://doi.org/10.1002/gj.954.

Çelik, O.F., Delaloye, M., Feraud, G., 2006. Precise ^{40}Ar–^{39}Ar ages from the metamorphic sole rocks of the Tauride Belt Ophiolites, southern Turkey: implications for the rapid cooling history. Geol. Mag. 143 (2), 213–227. https://doi.org/10.1017/S0016756805001524.

Chen, T., Jin, Z., Zhang, J., Wang, L., 2019. Calcium amphibole exsolution lamellae in chromite from the Semail ophiolite: evidence for a high-pressure origin. Lithos 334–335, 273–280. https://doi.org/10.1016/j.lithos.2019.03.020.

Collins, A.S., Robertson, A.H.F., 1998. Processes of Late Cretaceous to Late Miocene episodic thrust-sheet translation in the Lycian Taurides, SW Turkey. J. Geol. Soc., London 155 (5), 759–772. https://doi.org/10.1144/gsjgs.155.5.0759.

Cohen, A.S., Waters, F.G., 1996. Separation of osmium from geological materials by solvent extraction for analysis by thermal ionisation mass spectrometry. Anal. Chim. Acta 332 (2-3), 269–275. https://doi.org/10.1016/0003-2670(96)00226-7.

Creaser, R.A., Papanastassiou, D.A., Wasserburg, G.J., 1991. Negative thermal ion mass spectrometry of osmium, rhenium and iridium. Geochim. Cosmochim. Acta 55 (1), 397–401. https://doi.org/10.1016/0016-7037(91)90427-7.

D'Ippolito, V., Andreozzi, G.B., Bersani, D., Lottici, P.P., 2015. Raman fingerprint of chromate, aluminate and ferrite spinels. J. Raman Spectrosc. 46 (12), 1255–1264. https://doi.org/10.1002/jrs.4764.

Dick, H.J.B., Bullen, T., 1984. Chromian spinel as a petrogenetic indicator in abyssal and alpine-type peridotites and spatially associated lavas. Contrib Mineral Petr. 86 (1), 54–76. https://doi.org/10.1007/BF00373711.

Dilek, Y., Furnes, H., 2009. Structure and geochemistry of Tethyan ophiolites and their petrogenesis in subduction rollback systems. Lithos 113 (1-2), 1–20. https://doi.org/10.1016/j.lithos.2009.04.022.

Dilek, Y., Furnes, H., Shallo, M., 2007. Suprasubduction zone ophiolite formation along the periphery of Mesozoic Gondwana. Gondwana Res. 11 (4), 453–475. https://doi.org/10.1016/j.gr.2007.01.005.

Dilek, Y., Furnes, H., Shallo, M., 2008. Geochemistry of the Jurassic Mirdita Ophiolite (Albania) and the MORB to SSZ evolution of a marginal basin oceanic crust. Lithos 100 (1-4), 174–209. https://doi.org/10.1016/j.lithos.2007.06.026.

Dilek, Y., Rowland, J.C., 1993. Evolution of a conjugate passive margin pair in Mesozoic southern Turkey. Tectonics 12 (4), 954–970. https://doi.org/10.1029/93TC01060.

Dobrzhinetskaya, L.F., Wirth, R., Yang, J., Hutcheon, I.D., Weber, P.K., Green, H.W., 2009. High-pressure highly reduced nitrides and oxides from chromitite of a Tibetan ophiolite. Proc. Natl. Acad. Sci. USA 106 (46), 19233–19238. https://doi.org/10.1073/pnas.0905514106.

Droop, G.T.R., 1987. A general equation for estimating Fe^{3+} concentrations in ferromagnesian silicates and oxides from microprobe analyses, using stoichiometric criteria. Mineral. Mag. 51 (361), 431–435. https://doi.org/10.1180/minmag.1987.051.361.10.

Farré-de-Pablo, J., Proenza, J.A., González-Jiménez, J.M., Garcia-Casco, A., Colás, V., Roqué-Rossell, J., Camprubí, A., Sánchez-Navas, A., 2019. A shallow origin for diamonds in ophiolitic chromitites. Geology 47 (1), 75–78. https://doi.org/10.1130/G45640.1.

Farré-de-Pablo, J., Proenza, J.A., González-Jiménez, J.M., Aiglsperger, T., Garcia-Casco, A., Escuder-Viruete, J., Colás, V., Longo, F., 2020. Ophiolite hosted chromitite formed by supra-subduction zone peridotite – plume interaction. Geosci. Front. 11 (6), 2083–2102. https://doi.org/10.1016/j.gsf.2020.05.005.

Garuti, G., Fershtater, G., Bea, F., Montero, P., Pushkarev, E.V., Zaccarini, F., 1997. Platinum-group elements as petrological indicators in mafic-ultramafic complexes of the central and southern Urals: Preliminary results. Tectonophysics 276 (1-4), 181–194. https://doi.org/10.1016/S0040-1951(97)00050-4.

Gauthier, M., Corrivaux, L., Trottier, L.J., Cabri, J., Gilles Laflamme, J.H., Bergeron, M., 1990. Chromitites platinifères des complexes ophiolitiques de l'Estrie-Beauce, Appalaches du Sud du Québec. Miner. Deposita 25, 169–178. https://doi.org/10.1007/bf00190378.

Golubkova, A., Schmidt, M.W., Connolly, J.A.D., 2016. Ultra-reducing conditions in average mantle peridotites and in podiform chromitites: a thermodynamic model for moissanite (SiC) formation. Contrib. Mineral. Petrol. 171 (5), 41. https://doi.org/10.1007/s00410-016-1253-9.

Griffin, W.L., Afonso, J.C., Belousova, E.A., Gain, S.E., Gong, X.-H., González-Jiménez, J.M., Howell, D., Huang, J.-X., McGowan, N., Pearson, N.J., Satsukawa, T., Shi, R., Williams, P., Xiong, Q., Yang, J.-S., Zhang, M., O'Reilly, S.Y., 2016. Mantle recycling: Transition Zone metamorphism of Tibetan ophiolitic peridotites and its tectonic implications. J. Petrol. 57 (4), 655–684. https://doi.org/10.1093/petrology/egw011.

Harvey, J., Gannoun, A., Burton, K.W., Rogers, N.W., Alard, O., Parkinson, I.J., 2006. Ancient melt extraction from the oceanic upper mantle revealed by Re–Os isotopes in abyssal peridotites from the Mid-Atlantic ridge. Earth Planet. Sci. Lett. 244 (3-4), 606–621. https://doi.org/10.1016/j.epsl.2006.02.031.

Hickey, R.L., Frey, F.A., 1982. Geochemical characteristics of boninite series volcanics: implications for their source. Geochim. Cosmochim. Acta 46 (11), 2099–2115. https://doi.org/10.1016/0016-7037(82)90188-0.

Huang, E., Chen, C.H., Huang, T., Lin, E.H., Xu, J.-an., 2000. Raman spectroscopic characteristics of Mg-Fe-Ca pyroxenes. Am. Mineral. 85 (3-4), 473–479. https://doi.org/10.2138/am-2000-0408.

Huang, Y., Wang, L., Robinson, P.T., Ning, W., Zhong, Y., Wang, J., Hu, W., Polat, A., Kusky, T., 2021. Podiform chromitite genesis in an Archean juvenile forearc setting: The 2.55 Ga Zunhua chromitites, North China Craton. Lithos 394-395, 106194. https://doi.org/10.1016/j.lithos.2021.106194.

Jones, G., Robertson, A.H.F., 1991. Tectono-stratigraphy and evolution of the Mesozoic Pindos ophiolite and related units, northwestern Greece. J. Geol. Soc. 148 (2), 267–288. https://doi.org/10.1144/gsjgs.148.2.0267.

Juteau, T., Nicolas, A., Dubessy, J., Fruchard, J.C., Bouchez, J.L., 1977. Structural relationships in the Antalya ophiolite complex, Turkey: possible model for an oceanic ridge. Geol. Soc. Am. Bull. 1977 https://doi.org/10.1130/0016-7606(1977)88<1740:SRITAO>2.0.CO;2.

Kamenetsky, V.S., Crawford, A.J., Meffre, S., 2001. Factors controlling chemistry of magmatic spinel: an empirical study of associated olivine, Cr-spinel and melt inclusions from primitive rocks. J. Petrol. 42, 655–671. https://doi.org/10.1093/petrology/42.4.655.

Kato, Y., Fujinaga, K., Suzuki, K., 2005. Major and trace element geochemistry and Os isotopic composition of metalliferous umbers from the Late Cretaceous Japanese accretionary complex. Geochem. Geophys. Geosyst. 6 (7), n/a–n/a. https://doi.org/10.1029/2005GC000920.

Korsakov, A.V., Vandenabeele, P., Theunissen, K., 2005. Discrimination of metamorphic diamond populations by Raman spectroscopy (Kokchetav, Kazakhstan). Spectrochim. Acta A Mol. Biomol. Spectroscopy 61 (10), 2378–2385. https://doi.org/10.1016/j.saa.2005.02.016.

Kusky, T., Wang, L., Robinson, P.T., Huang, Y., Wirth, R., Ning, W., Zhong, Y., Polat, A., 2021. Ultra-high pressure inclusion in Archean ophiolitic podiform chromitite in mélange block suggests deep subduction on early Earth. Precambr. Res. 362, 106318. https://doi.org/10.1016/j.precamres.2021.106318.

Kusky, T., Huang, Y., Wang, L., Robinson, P.T., Wirth, R., Polat, A., Wei, H., 2022. Vestiges of early Earth's deep subduction and CHONSP cycle recorded in Archean ophiolitic podiform chromitites. Earth-Sci. Rev. 227, 103968. https://doi.org/10.1016/j.earscirev.2022.103968.

Lapierre, H., Samper, A., Bosch, D., Maury, R., Bechennec, F., Cotten, J., Demant, A., Brunet, P., Keller, F., Marcoux, J., 2004. The Tethyan plume: geochemical diversity of Middle Permian basalts from the Oman rifted margin. Lithos 74, 167–198. https://doi.org/10.1016/j.lithos.2004.02.006.

Lay, A., Graham, I., Cohen, D., Privat, K., González-Jiménez, J.M., Belousova, E., Barnes, S.-J., 2017. Ophiolitic chromitites of Timor Leste: their composition, platinum group element geochemistry, mineralogy, and evolution. Canad. Mineral. 55 (5), 875–908. https://doi.org/10.3749/canmin.1500032.

Leblanc, M., Nicolas, A., 1992. Ophiolitic chromitites. Int. Geol. Rev. 34 (7), 653–686. https://doi.org/10.1080/00206819209465629.

Lenaz, D., Lughi, V., 2013. Raman study of $MgCr_2O_4$-$Fe^{2+}Cr_2O_4$and $MgCr_2O_4$-$MgFe^{3+}_2O_4$ synthetic series: the effects of Fe^{2+} and Fe^{3+}on Raman shifts. Phys. Chem. Miner. 40 (6), 491–498. https://doi.org/10.1007/s00269-013-0586-4.

Lenaz, D., Lughi, V., 2017. Raman spectroscopy and the inversion degree of natural Cr-bearing spinels. Am. Mineral. 102, 327–332. https://doi.org/10.2138/am-2016-5814.

Li, J., Liang, X.R., Xu, J.F., Suzuki, K., Dong, Y.H., 2010a. Simplified technique for the measurementsof Re–Os isotope by multicollector inductively coupled plasma mass spectrometry (MC-ICP-MS). Geochem. J. 44 (1), 73–80. https://doi.org/10.2343/geochemj.1.0044.

Li, J., Xu, J.-F., Suzuki, K., He, B., Xu, Y.-G., Ren, Z.-Y., 2010b. Os, Nd and Sr isotope and trace element geochemistry of the Muli picrites: insights into the mantle source of the Emeishan Large Igneous Province. Lithos 119 (1-2), 108–122. https://doi.org/10.1016/j.lithos.2010.06.002.

Lian, D.Y., Yang, J.S., Dilek, Y., Wu, W.W., Zhang, Z.M., Xiong, F.H., Liu, F., Zhou, W.D., 2017. Deep mantle origin and ultra-reducing conditions in podiform chromitite: Diamond, moissanite and other unusual minerals in podiform chromitties from the Pozanti-Karsanti ophiolite, southern Turkey. Am. Mineral. 102, 1101–1113. https://doi.org/10.2138/am-2017-5850.

Liu, C.-Z., Snow, J.E., Hellebrand, E., Brügmann, G., von der Handt, A., Büchl, A., Hofmann, A.W., 2008. Ancient, highly heterogeneous mantle beneath Gakkel ridge, Arctic Ocean. Nature 452 (7185), 311–316. https://doi.org/10.1038/nature06688.

Liu, C.-Z., Zhang, C., Yang, L.-Y., Zhang, L.-L., Ji, W.-Q., Wu, F.-Y., 2014. Formation of gabbronorites in the Purang ophiolite (SW Tibet) through melting of hydrothermally altered mantle along a detachment fault. Lithos 205, 127–141. https://doi.org/10.1016/j.lithos.2014.06.019.

Liu, F., Lian, D., Wu, W., Yang, J., 2021. Diamond and other exotic mineral-bearing ophiolites on the globe: a key to understand the discovery of new minerals and formation of ophiolitic podiform chromitite. Crystals 2021 (11), 1362. https://doi.org/10.3390/cryst11111362.

Liu, X., Su, B.-X., Bai, Y., Robinson, P.T., Tang, X., Xiao, Y., Xue, D.-S., Cui, M.-M., 2020. Genesis of "silicate exsolution lamellae" in chromite of the Stillwater Complex: A challenge to the high-pressure crystallization of ophiolitic chromitite. Lithos 378-379, 105796. https://doi.org/10.1016/j.lithos.2020.105796.

Machev, P., O'Bannon, E.F., Bozhilov, K.N., Wang, Q., Dobrzhinetskaya, L., 2018. Not all moissanites are created equal: New constraints on moissanite from metamorphic rocks of Bulgaria. Earth Planet. Sci. Lett. 498, 387–396. https://doi.org/10.1016/j.epsl.2018.07.009.

Marchesi, C., González-Jiménez, J.M., Gervilla, F., Garrido, C.J., Griffin, W.L., O'Reilly, S.Y., Proenza, J.A., Pearson, N.J., 2011. In situ Re–Os isotopic analysis of platinum-group minerals from the Mayarí-Cristal ophiolitic massif (Mayarí–Baracoa Ophiolitic Belt, eastern Cuba): implications for the origin of Os-isotope heterogeneities in podiform chromitites. Contrib. Mineral. Petrol. 161 (6), 977–990. https://doi.org/10.1007/s00410-010-0575-2.

McGowan, N.M, Griffin, W.L., González-Jiménez, J.M., et al., 2015. Tibetan chromitites: Excavating the slab graveyard. Geology 43(2), 179–182. https://doi.org/10.1130/G36245.1.

McInnes, B.I.A., McBride, J.S., Evans, N.J., Lambert, D.D., Andrew, A.S., 1999. Osmium isotope constraints on ore metal recycling in subduction zones. Science 286 (5439), 512–516. https://doi.org/10.1126/science:286.5439.512.

Meisel, T., Moser, J., Wegscheider, W., 2001. Recognizing heterogeneous distribution of platinum group elements (PGE) in geological materials by means of the Re–Os isotope system. Fresenius' J. Anal. Chem. 370, 566–572. https://doi.org/10.1007/s002160100791.

Moreno, T., Gibbons, W., Prichard, H.M., Lunar, R., 2001. Platiniferous chromitite and the tectonic setting of ultramafic rocks in Cabo Ortegal, NW Spain. Journal of the Geological Society 158 (4), 601–614. https://doi.org/10.1144/jgs.158.4.601.

Morishita, T., Arai, S., 2003. Evolution of spinel–pyroxene symplectite in spinel lherzolites from the Horoman Complex, Japan. Contrib. Mineral. Petrol. 144, 509–522. https://doi.org/10.1144/jgs.158.4.601.

Najafzadeh, A.R., Ahmadipour, H., 2014. Using platinum-group elements and Au geochemistry to constrain the genesis of podiform chromitites and associated peridotites from the Soghan mafic–ultramafic complex, Kerman, Southeastern Iran. Ore Geol. Rev. 60, 60–75. https://doi.org/10.1016/j.oregeorev.2013.12.014.

Nakamura, M., 1995. Residence time and crystallization history of nickeliferous olivine phenocrysts from northern Yatsugatake volcanoes, central Japan: Application of a growth and diffusion model in the system Mg-Fe-Ni. J. Volcanol. Geoth. Res. 66, 81–100. https://doi.org/10.1016/0377-0273(94)00054-K.

Nier, A.O., 1950. A redetermination of the relative abundances of the isotopes of carbon, nitrogen, oxygen, argon and potassium. Phys. Rev. B 77 (6), 789–793. https://doi.org/10.1103/PhysRev.77.789.

Ning, W., Kusky, T., Wang, J., Wang, L., Deng, H., Polat, A., Huang, B., Peng, H., Feng, P., 2020. From subduction initiation to arc-polarity reversal: Life cycle of an Archean subduction zone from the Zunhua ophiolitic mélange, North China Craton. Precambrian Res. 350, 105868. https://doi.org/10.1016/j.precamres.2020.105868.

Okay, A.I., Tansel, I., Tuysuz, O., 2001. Obduction, subduction and collision as reflected in the Upper Crateceous-Lower Eocene sedimentary record of western Turkey. Geol. Mag. 138, 1171–1242. https://doi.org/10.1017/S0016756801005088.

Ozawa, K., 1994. Melting and melt segregation in the mantle wedge above a subduction zone: evidence from the chromite-bearing peridotites of the Miyamori Ophiolite Complex, northeastern Japan. J. Petrol. 35 (3), 647–678. https://doi.org/10.1093/petrology/35.3.647.

Pagé, P., Barnes, S.J., 2009. Using trace-elements in chromites to constrain the origin of podiform chromitites in the Thetford Mines Ophiolite, Québec. Canada. Econ. Geol. 104, 997–1018. https://doi.org/10.2113/gsecongeo.104.7.997.

Pagé, P., Bédard, J.H., Schroetter, J.-M., Tremblay, A., 2008. Mantle petrology and mineralogy of the Thetford Mines ophiolite complex. Lithos 100 (1-4), 255–292. https://doi.org/10.1016/j.lithos.2007.06.017.

Parlak, O., Dunkl, I., Karaoglan, F., Kusky, T.M., Zhang, C., Wang, L., Koepke, J., Billor, Z., Hames, W.E., Şimşek, E., Şimşek, G., Şimşek, T., Ezgi Öztürk, S., 2019. Rapid cooling of a Neotehtyan ophiolite: evidence for contemporaneous subduction initiation and metamorphic sole formation. Geol. Soc. Am. Bull. 131, 2011–2038. https://doi.org/10.1130/B35040.1.

Pearson, D.G., Woodland, S.J., 2000. Solvent extraction/anion exchange separation and determination of PGEs (Os, Ir, Pt, Pd, Ru) and Re–Os isotopes in geological samples by isotope dilution ICP–MS. Chem. Geol. 165 (1-2), 87–107. https://doi.org/10.1016/S0009-2541(99)00161-8.

Piccardo, G.B., Zanetti, A., Müntener, O., 2007. Melt/peridotite interaction in the Lanzo South peridotite: field, textural and geochemical evidence. Lithos 94, 181–209. https://doi.org/10.1016/j.lithos.2006.07.002.

Prichard, H.M., Neary, C.R., Fisher, P.C., O'Hara, M.J., 2008. PGE-rich podiform chromitites in the Al'Ays ophiolite complex, Saudi Arabia: an example of critical mantle melting to extract and concentrate PGE. Econ. Geol. 103 (7), 1507–1529. https://doi.org/10.2113/gsecongeo.103.7.1507.

Pujol-Solà, N., Domínguez-Carretero, D., Proenza, J.A., Haissen, F., Ikenne, M., González-Jiménez, J.M., Colás, V., Maacha, L., Garcia-Casco, A., 2021. The chromitites of the Neoproterozoic Bou Azzer ophiolite (central Anti-Atlas, Morocco) revisited. Ore Geol. Rev. 134, 104166. https://doi.org/10.1016/j.oregeorev.2021.104166.

Pujol-Solà, N., Garcia-Casco, A., Proenza, J.A., González-Jiménez, J.M., Campo, A., Colás, V., Canáls, A., Sánchez-Navas, A., Roqué-Rosell, J., 2020. Diamond forms during low pressure serpentinisation of oceanic lithosphere. Geochem. Perspect. 15, 19–24. https://doi.org/10.7185/geochemlet.2029.

Pujol-Solà, N., Proenza, J., Garcia-Casco, A., González-Jiménez, J., Andreazini, A., Melgarejo, J., Gervilla, F., 2018. An alternative scenario on the origin of ultra-high pressure (Uhp) and super-reduced (sur) minerals in ophiolitic chromitites: a case study from the mercedita deposit (eastern cuba). Minerals 8 (10), 433. https://doi.org/10.3390/min8100433.

Rassios, A.E., Dilek, Y., 2009. Rotational deformation in the Jurassic Mesohellenic ophiolites, Greece, and its tectonic significance. Lithos 108 (1-4), 207–223. https://doi.org/10.1016/j.lithos.2008.09.005.

Reisberg, L., Lorand, J.-P., Bedini, R.M., 2004. Reliability of Os model ages in pervasively metasomatized continental mantle lithosphere: a case study of Sidamo magnesiochromite peridotite xenoliths (East African Rift, Ethiopia). Chem. Geol. 208, 119–140. https://doi.org/10.1016/j.chemgeo.2004.04.008.

Robertson, A.H.F., 2002. Overview of the genesis and emplacement of Mesozoic ophiolites in the Eastern Mediterranean Tethyan region. Lithos 65 (1-2), 1–67. https://doi.org/10.1016/S0024-4937(02)00160-3.

Roy-Barman, M., 1993. Measure du Rapport $^{187}Os/^{188}Os$ Dans les Basaltes et les Peridotites: Contribution a la Systematique $^{187}Re–^{187}Os$ Dans le Manteau. Ph.D. Thesis. Universite de Paris VII.

Rudnick, R.L., Walker, R.J., 2009. Interpreting ages from Re–Os isotopes in peridotites. Lithos 112, 1083–1095. https://doi.org/10.1016/j.lithos.2009.04.042.

Rui, H.-C., Yang, J.-S., Llanes Castro, A.I., Zheng, J.-P., Lian, D.-Y., Wu, W.-W., Valdes Mariño, Y., 2022. Ti-poor high-Al chromitites of the Moa-Baracoa ophiolitic massif (eastern Cuba) formed in a nascent forearc mantle. Ore Geol. Rev. 144, 104847. https://doi.org/10.1016/j.oregeorev.2022.104847.

Satsukawa, T., Griffin, W.L., Piazolo, S., O'Reilly, S.Y., 2015. Messengers from the deep: Fossil wadsleyite–chromite microstructures from the Mantle Transition Zone. Sci. Rep. 5, 16484. https://doi.org/10.1038/srep16484.

Schmidt, M.W., Gao, C., Golubkova, A., Rohrbach, A., Connolly, J.A., 2014. Natural moissanite (SiC) - a low temperature mineral formed from highly fractionated ultra-reducing COH-fluids. Prog. Earth Planet. Sci. 1 (1), 1–14. https://doi.org/10.1186/s40645-014-0027-0.

Shi, R., Alard, O., Zhi, X., O'Reilly, S.Y., Pearson, N.J., Griffin, W.L., Zhang, M., Chen, X., 2007. Multiple events in the Neo-Tethyan oceanic upper mantle: evidence from Ru–Os–Ir alloys in the Luobusa and Dongqiao ophiolitic podiform chromitites, Tibet. Earth Planet. Sci. Lett. 261 (1-2), 33–48. https://doi.org/10.1016/j.epsl.2007.05.044.

Shiraki, K., 1997. Geochemical behavior of chromium. Resour. Geol. 47, 319–330. https://doi.org/10.11456/shigenchishitsu1992.47.319.

Shirey, S.B., Walker, R.J., 1995. Carius tube digestion for low-blank rhenium–osmium analysis. Anal. Chem. 67 (13), 2136–2141. https://doi.org/10.1021/ac00109a036.

Su, B.X., Teng, F.Z., Hu, Y., Shi, R.D., Zhou, M.F., Zhu, B., Liu, F., Gong, X.H., Huang, Q. S., Xiao, Y., Chen, C., He, Y.S., 2015. Iron and magnesium isotope fractionationin oceanic lithosphere and sub-arc mantle: perspectives from ophiolites. Earth Planet. Sci. Lett. 430, 523–532. https://doi.org/10.1016/j.epsl.2015.08.020.

Sun, Y., Sun, M., 2005. Nickel sulfide fire assay improved for pre-concentration of platinum group elements in geological samples: a practical means of ultra-trace analysis combined with inductively coupled plasma-mass spectrometry. Analyst 130, 664-669. https://doi.org/10.1039/b416844e.

Suzuki, K., Honda, M., 2003. Analytical procedure for osmium and rhenium isotopes. Front. Res. Earth Evol. 1, 379–381. https://doi.org/10.2343/geochemj.40.297.

Suzuki, K., Miyata, Y., Kanazawa, N., 2004. Precise Re isotope ratio measurements bynegative thermal ionization mass spectrometry (NTI-MS) using total evaporation technique. Int. J. Mass Spectrom. 235 (1), 97–101. https://doi.org/10.1016/j.ijms.2004.04.006.

Takahashi, E., 1986. Origin of basaltic magmas: implications from peridotite melting experiments and olivine fractionation model. Bull. Volcanol. Soc. Japan 30, 517–540 (in Japanese).

Tubía, J.M., Cuevas, J., Esteban, J.J., 2004. Tectonic evidence in the Ronda peridotites, Spain, for mantle diapirism related to delamination. Geology 32, 941–944. https://doi.org/10.1130/G20869.1.

Trumbull, R.B., Yang, J.-S., Robinson, P.T., Di Pierro, S., Vennemann, T., Wiedenbeck, M., 2009. The carbon isotope composition of natural SiC (moissanite) from the Earth's mantle: New discoveries from ophiolites. Lithos 113 (3-4), 612–620. https://doi.org/10.1016/j.lithos.2009.06.033.

Uysal, I., Kapsiotis, A., Akmaz, R.M., Saka, S., Seitz, H.M., 2018. The Guleman ophiolitic chromitites (SE Turkey) and their link to a compositionally evolving mantle source during subduction initiation. Ore Geol. Rev. 93, 98–113. https://doi.org/10.1016/j.oregeorev.2017.12.017.

Uysal, I., Akmaz, R.M., Saka, S., Kapsiotis, A., 2016. Coexistence of compositionally heterogeneous chromitites in the Antalya-Isparta ophiolitic suite, SW Turkey: A record of sequential magmatic processes in the sub-arc lithospheric mantle. Lithos 248–251, 160–174. https://doi.org/10.1016/j.lithos.2016.01.021.

Uysal, I., Ersoy, E.Y., Karsli, O., Dilek, Y., Sadiklar, M.B., Ottley, C.J., Tiepolo, M., Meisel, T., 2012. Coexistence of abyssal and ultra-depleted SSZ type mantle peridotites in a Neo-Tethyan ophiolite in SW Turkey: constraints from mineral composition, whole-rock geochemistry (major-trace-REE-PGE), and Re-Os isotope systematics. Lithos 132–133, 50–69. https://doi.org/10.1016/j.lithos.2011.11.009.

Uysal, I., Sadiklar, M., Tarkian, M., Karsli, O., Aydin, F., 2005. Mineralogy and composition of the chromitites and their platinum-group minerals from Ortaca (Muğla-SW Turkey): evidence for ophiolitic chromitite genesis. Mineral. Petrol. 83, 219–242. https://doi.org/10.1007/s00710-004-0063-3.

Uysal, I., Tarkian, M., Sadiklar, M.B., Sen, C., 2007. Platinum-group-element geochemistry and mineralogy of ophiolitic chromitites from the Kop mountains, Northeastern Turkey. Can. Mineral. 45 (2), 355–377. https://doi.org/10.2113/gscanmin.45.2.355.

Uysal, İ., Tarkian, M., Sadiklar, M.B., Zaccarini, F., Meisel, T., Garuti, G., Heidrich, S., 2009. Petrology of Al- and Cr-rich ophiolitic chromitites from the Muğla, SW Turkey: implications from composition of chromite, solid inclusions of platinum-group mineral, silicate, and base-metal mineral, and Os-Isotope geochemistry. Contrib Mineral Petr. 158 (5), 659–674. https://doi.org/10.1007/s00410-009-0402-9.

Völkening, J., Walczyk, T., Heumann, K.G., 1991. Osmium isotope ratio determinations by negative thermal ionization mass spectrometry. Int. J. Mass Spectrom. Ion Processes 105 (2), 147–159. https://doi.org/10.1016/0168-1176(91)80077-Z.

Walker, R., Carlson, R., Shirey, S., 1989. Os, Sr, Nd, and Pb isotope systematics of southern African peridotite xenoliths: implications for the chemical evolution of subcontinental mantle. Geochim. Cosmochim. Acta 53, 1583–1595. https://doi.org/10.1016/0016-7037(89)90240-8.

Walker, R.J., Prichard, H.M., Ishiwatari, A., Pimentel, M., 2002. The osmium isotopic composition of convecting upper mantle deduced from ophiolite chromites. Geochim. Cosmochim. Acta 66 (2), 329–345. https://doi.org/10.1016/S0016-7037(01)00767-0.

Widom, E., Kepezhinskas, P., Defant, M., 2003. The nature of metasomatism in the sub-arc mantle wedge: evidence from Re–Os isotopes in Kamchatka peridotite xenoliths. Chem. Geol. 196 (1-4), 283–306. https://doi.org/10.1016/S0009-2541(02)00417-5.

Xiong, F., Liu, Z., Kapsiotis, A., Yang, J., Lenaz, D., Robinson, P.T., 2019. Petrogenesis of lherzolites from the Purang ophiolite, Yarlung-Zangbo Suture Zone, Tibet: origin and significance of ultra-high pressure and other "unusual" minerals in the Neo-Tethyan lithospheric mantle. Int. Geol. Rev. 61 (17), 2184–2210. https://doi.org/10.1080/00206814.2019.1584771.

Xiong, F.H., Yang, J., Xua, X., Kapsiotis, A., Hao, X., Liu, Z., 2018a. Compositional and isotopic heterogeneities in the Neo-Tethyan upper mantle recorded by coexisting Al-rich and Cr-rich chromitites in the Purang peridotite massif, SW Tibet (China). J. Asian Earth Sci. 159, 109–129. https://doi.org/10.1016/j.jseaes.2018.03.024.

Xiong, F.H., Yang, J.S., Dilek, Y., et al., 2018b. Petrology and geochemistry of the high-Cr podiform chromitites of the Köyceğiz ophiolite, southwest Turkey: implications for the multi-stage evolution of the oceanic upper mantle. Mineral. Petrol. 112, 685–704. https://doi.org/10.1007/s00710-018-0560-4.

Xiong, F., Yang, J., Robinson, P.T., Xu, X., Liu, Z., Li, Y., Li, J., Chen, S., 2015a. Origin of podiform chromitite, a new model based on the Luobusa ophiolite, Tibet. Gondwana Res. 27 (2), 525–542. https://doi.org/10.1016/j.gr.2014.04.008.

Xiong, F.H., Yang, J.S., Robinson, P.T., Dilek, Y., Milushi, I., Xu, X.Z., Chen, Y.H., Zhou, W.D., Zhang, Z.M., Lai, S.M., Tian, Y.Z., Huang, Z., 2015b. Petrology and geochemistry of high Cr podiform chromitites of Bulqiza, Eastern Mirdita Ophiolite (EMO), Albania. Ore Geology Review 70, 188–207. https://doi.org/10.1016/j.oregeorev.2015.04.011.

Xiong, F., Yang, J., Robinson, P.T., Xu, X., Liu, Z., Zhou, W., Feng, G., Xu, J., Li, J., Niu, X., 2017. High-Al and high-Cr podiform chromitites from the western Yarlung-Zangbo suture zone, Tibet: implications from mineralogy and geochemistry of chromian spinel, and platinum-group elements. Ore Geology Rev. 80, 1020–1041. https://doi.org/10.1016/j.oregeorev.2016.09.009.

Xiong, F.H., Xu, X.Z., Mugnaioli, E., Gemmi, M., Wirth, R., Yang, J.S., Grew, E.S., 2022a. Wenjiite, Ti10(Si,P,)$_7$, and kangjinlaite, $Ti_{11}Si_{10}$, new minerals in the ternary Ti-P-Si system from the Luobusa ophiolite, Tibet, China. Am. Mineral., https://doi.org/10.2138/am-2022-8226.

Xiong, F.H., Xu, X.Z., Mugnaioli, E., Gemmi, M., Wirth, R., Grew, E.S., Robinson, P.T., 2022b. Jingsuiite, TiB_2, a new mineral from the Cr-11 podiform chromitite orebody, Luobusa ophiolite, Tibet, China: Implications for recycling of boron. Am. Mineral. 107, 43–53. https://doi.org/10.2138/am-2021-7647.

Xiong, F.H., Zoheir, B., Wirth, R., Milushi, I., Qiu, T., Yang, J.S., 2021. Mineralogical and isotope peculiarities of high-Cr chromitites: implications for a mantle convection genesis of the Bulqiza ophiolite. Lithos, 398–399, 106305. https://doi.org/10.1016/j.lithos.2021.106305.

Xu, X.Z., Yang, J.S., Chen, S.Y., Fang, Q.S., Bai, W.J., Ba, D.Z., 2009. Unusual mantle mineral group from chromitite orebody Cr-11 in Luobusa ophiolite of Yarlung-Zangbo suture zone, Tibet. J. Earth Sci. 20 (2), 284–302. https://doi.org/10.1007/s12583-009-0026-z.

Xu, X.Z., Yang, J.S., Guo, G.L., Li, J.Y., 2011. Lithological research on the Purang mantle peridotite in western Yarlung-Zangbo suture zone in Tibet. Acta Petrol. Sinica 27, 3179–3196 (in Chinese with English abstract).

Yamamoto, S., Komiya, T., Hirose, K., Maruyama, S., 2009. Coesite and clinopyroxene exsolution lamellae in chromites: In-situ ultrahigh-pressure evidence from podiform chromitites in the Luobusa ophiolite, southern Tibet. Lithos 109 (3-4), 314–322. https://doi.org/10.1016/j.lithos.2008.05.003.

Yang, J.S., Xiong, F.H., Guo, G.L., Liu, F., Liang, F.H., Chen, S.Y., Li, Z.L., Zhang, L.W., 2011. The Dongbo ultramafic massif: A mantle peridotite in the western part of the Yarlung Zangbo suture zone, Tibet, with excellent prospects for a major chromite deposit. Acta Petrol. Sinica 27 (11), 3207–3222 (in Chinese with English abstract).

Yang, J., Meng, F., Xu, X., Robinson, P.T., Dilek, Y., Makeyev, A.B., Wirth, R., Wiedenbeck, M., Cliff, J., 2015. Diamonds, native elements and metal alloys from chromitites of the Ray-Iz ophiolite of the Polar Urals. Gondwana Res. 27 (2), 459–485. https://doi.org/10.1016/j.gr.2014.07.004.

Yang, J.-S., Dobrzhinetskaya, L., Bai, W.-J., Fang, Q.-S., Robinson, P.T., Zhang, J., Green, H.W., 2007. Diamond-and coesite-bearing chromitites from the Luobusa ophiolite. Tibet. Geology 35 (10), 875. https://doi.org/10.1130/G23766A.110.1130/2007220.

Yang, J.S., Robinson, P.T., Dilek, Y., 2014. Diamonds in Ophiolites: a little – known diamond occurrence. Elements 10, 123–126. https://doi.org/10.2113/gselements.10.2.123.

Yang, J.S., Wu, W.W., Lian, D.Y., Rui, H.C., 2021. Peridotites, chromitites and diamonds in ophiolites. Nat. Rev. Earth Environ. 2 (3), 198–212. https://doi.org/10.1038/s43017-020-00138-4.

Yin, A., Harrison, T.M., 2000. Geologic evolution of the Himalayan-Tibetan orogen. Annu. Rev. Earth Planet. Sci. 28 (1), 211–280. https://doi.org/10.1146/earth.2000.28.issue-110.1146/annurev.earth.28.1.211.

Zhou, M.F., Robinson, P.T., Malpas, J., Edwards, S.J., Qi, L., 2005. REE and PGE geochemical constraints on the formation of dunites in the Luobusa ophiolite, southern Tibet. J. Petrol. 46, 615–639. https://doi.org/10.1093/petrology/egh091.

Zhou, M.F., Robinson, P.T., Su, B.X., Gao, J.F., Li, J.W., Yang, J.S., Malpas, J., 2014. Compositions of chromite, associated minerals, and parental magmas of podiform chromite deposits: The role of slab contamination of asthenospheric melts in suprasubduction zone envrionments. Gondwana Res. 26 (1), 262–283. https://doi.org/10.1016/j.gr.2013.12.011.

Zhou, M.-F., Sun, M., Keays, R.R., Kerrich, R.W., 1998. Controls on platinum–group elemental distributions of podiform chromitites: a case study of high–Cr and high–Al chromitites from Chinese orogenic belts. Geochim. Cosmochim. Acta 62 (4), 677–688. https://doi.org/10.1016/S0016-7037(97)00382-7.

Zhou, X., Zheng, J., Li, Y., Griffin, W.L., Xiong, Q., Moghadam, H.S., O'Reilly, S.Y., 2019. Neoproterozoic sedimentary rocks track the location of the Lhasa Block during the Rodinia breakup. Precambr. Res. 320, 63–77. https://doi.org/10.1016/j.precamres.2018.10.005.